INFERRING STRUCTURE-FUNCTION RELATIONS FROM CONNECTOME DATA:

INSIGHTS FROM A CASE STUDY OF THE MACAQUE BRAIN

Shakti N. Menon

The Institute of Mathematical Sciences, Chennai

May 27th 2025

Brains, Dynamics & Computation: A Workshop on Network Neuroscience

PART I: THE BRAINY PRIMATE

image: Ken Kwapis, "Dunston Checks In" (1996)

The CoCoMac (Collation of Connectivity data on the Macaque brain) database was an initiative of Rolf Kötter that began in the late 1990s.

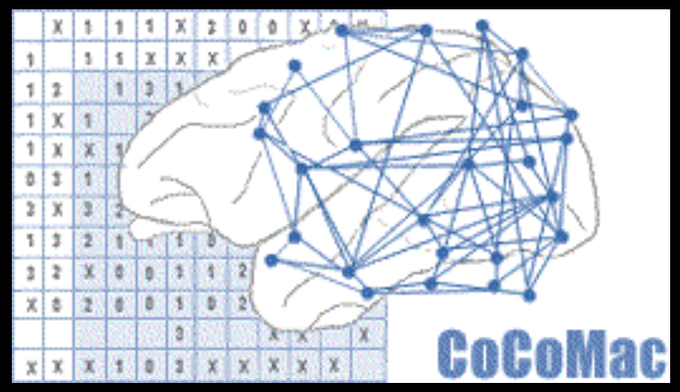

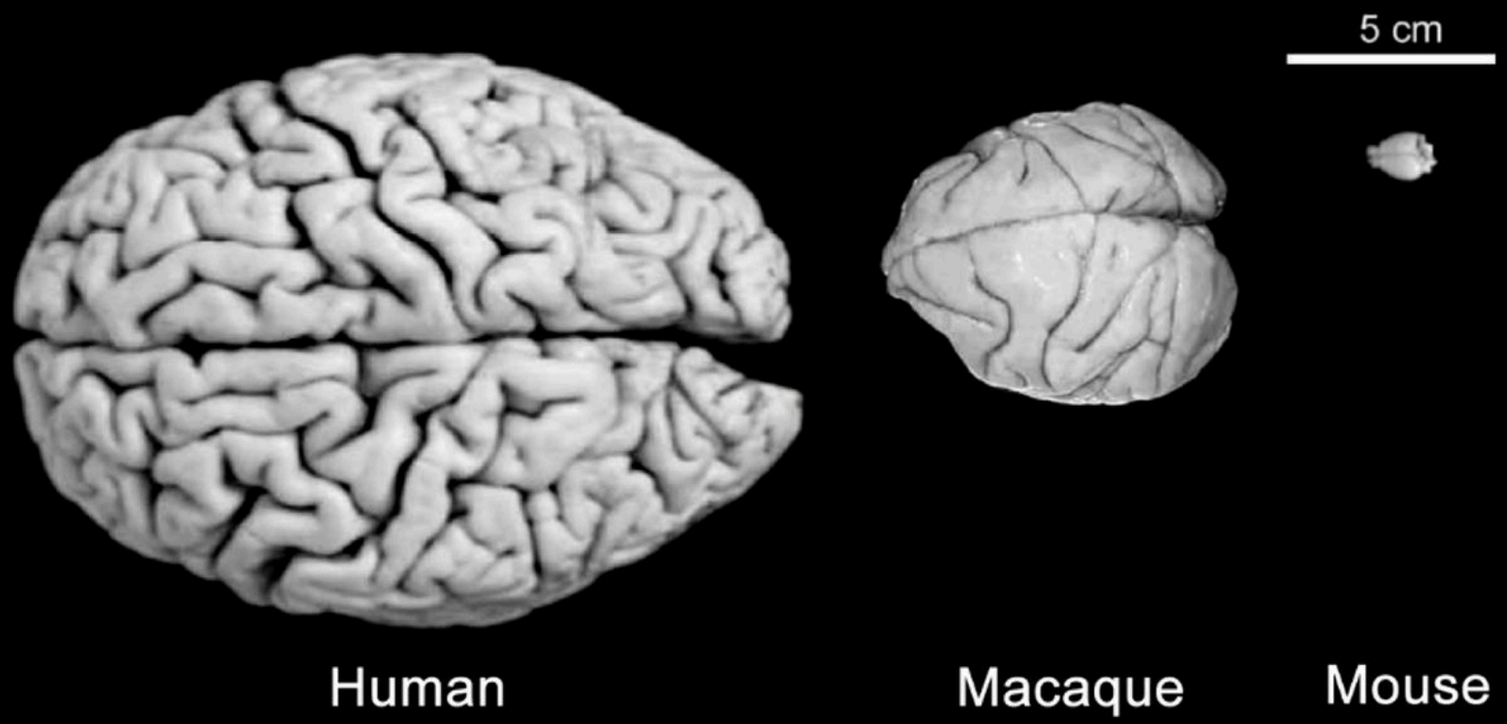

This database collates information from hundreds of axonal tract-tracing studies to provide a comprehensive record of the wiring of the primate brain.

The advantages of tract-tracing is that it provides incontrovertible evidence of long-range connections, as well as the associated directionality.

image: DT Gray & CA Barnes, *PNAS* **116**(52), 26247 (2019).

Network of connections in the Macaque brain

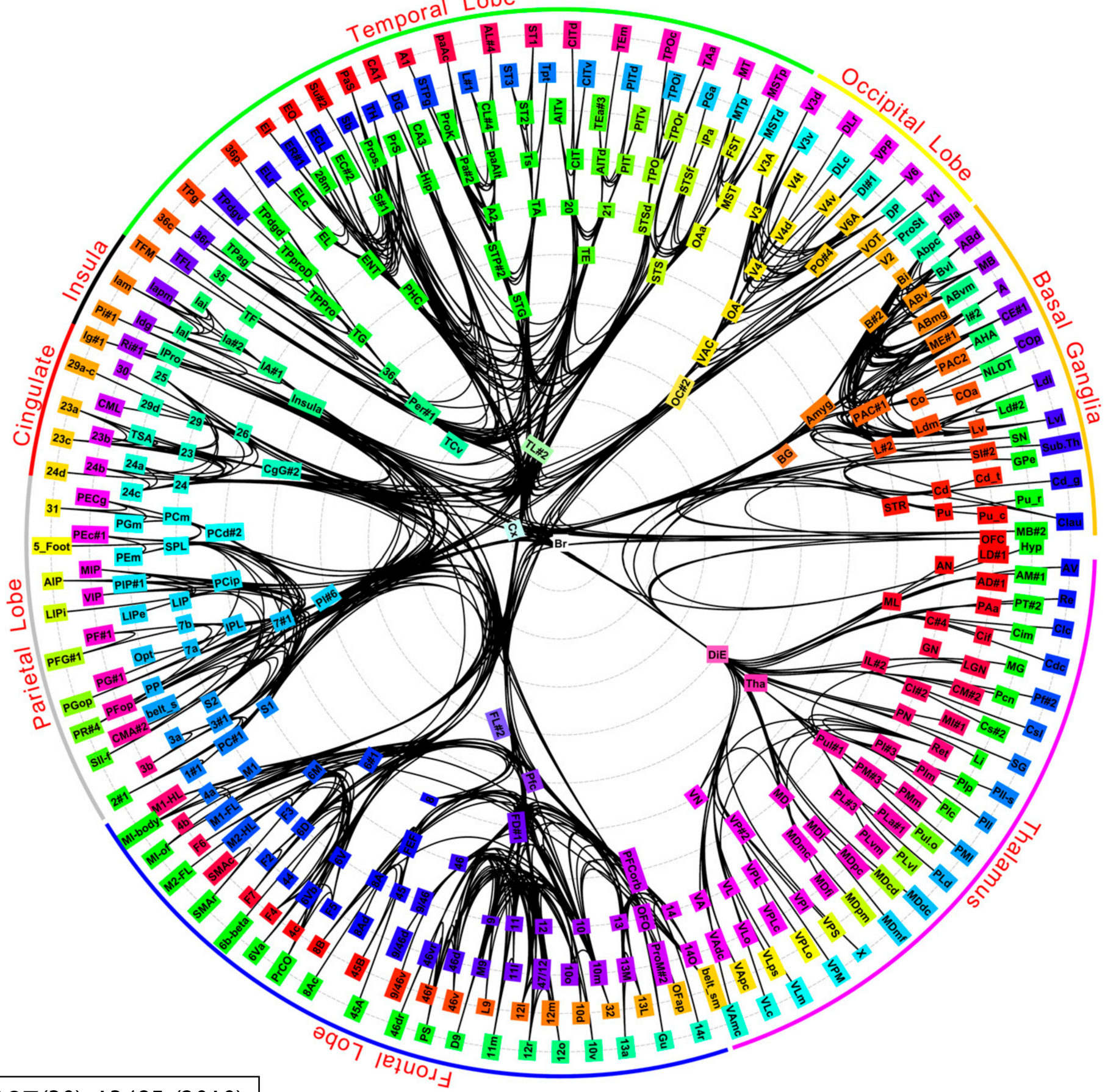

image: DS Modha & R Singh, *PNAS* **107**(30), 13485 (2010).

BRAIN REGIONS IN THE MODHA & SINGH NETWORK

Table S1: Hierarchical brain map in depth-first order

Level	Acronym	Full Name [Merged Brain Regions]	Ring Number	Degree	Number of times studied	Number of Connections reported
0	Br	Brain according to GM-Definition	0	0	3	0
1	DiE	Diencephalon according to GM-Definition	4	0	1	0
2	Hyp	Hypthalamus [ALH APH DMH Hce1 Hce2 SMH hy]	10	25	9	50
2	Tha	Thalamus	5	1	2	1
3	AN	Anterior nuclei of the thalamus [LN]	8	8	6	11
4	LD#1	Laterodorsal nucleus (thalamus) [Cld]	9	14	17	15
4	AV	Nucleus anterior ventralis thalami	11	7	15	7
4	AM#1	Nucleus anterior medialis thalami [AMdc]	10	22	16	23
4	AD#1	Nucleus anterior dorsalis thalami	9	5	10	5
3	ML	Midline nuclei of the thalamus [Pac#2 sPFmc sPFpc]	7	12	14	18
4	Re	Nucleus reuniens thalami [Rv]	11	24	14	26
4	PT#2	Nucleus parataenialis thalami	10	7	5	7
4	PAa	Nucleus paraventricularis thalami, pars anterior [PAm#2 PAp Pa#3]	9	13	13	16
4	C#4	Nucleus centralis thalami [Ce#2 CeM#2]	8	4	4	4
5	Clc	Nucleus centralis latocellularis thalami	11	11	7	12
5	Cim	Nucleus centralis intermedialis thalami	10	7	5	7
5	Cif	Nucleus centralis inferior thalami	9	11	8	11
5	Cdc	Nucleus centralis densocellularis thalami [ND]	11	17	10	19
3	GN	Metathalamus (Geniculate Nuclei)	8	0	1	0
4	MG	Corpus geniculatum mediale [AD#3 GM GMpc MC MGM MGN MGad] [MGpd PD#3 V Z]	10	23	59	49
4	LGN	dorsal Lateral geniculate nucleus [2#2 DLG DLGN LGN#1 LGN_0 LGN_1] [LGN_2 LGN_3 LGN_4 LGN_5 LGN_6 LGN_il LGN_il-z] [LGN_k1 LGN_l LGN_mc LGN_mc-il LGN_mc-l LGN_pc LGN_pc-il] [LGN_pc-l LGN_s LGd LGm LGp LGv]	9	10	78	86
3	IL#2	Intralaminar nuclei of the thalamus	7	14	5	14
3	PrC	Nucleus prethalamicus (prethalamus)	11	12	13	13

image: DS Modha & R Singh, *PNAS* **107**(30), 13485 (2010)

CREATING A "LEAF NODE" NETWORK

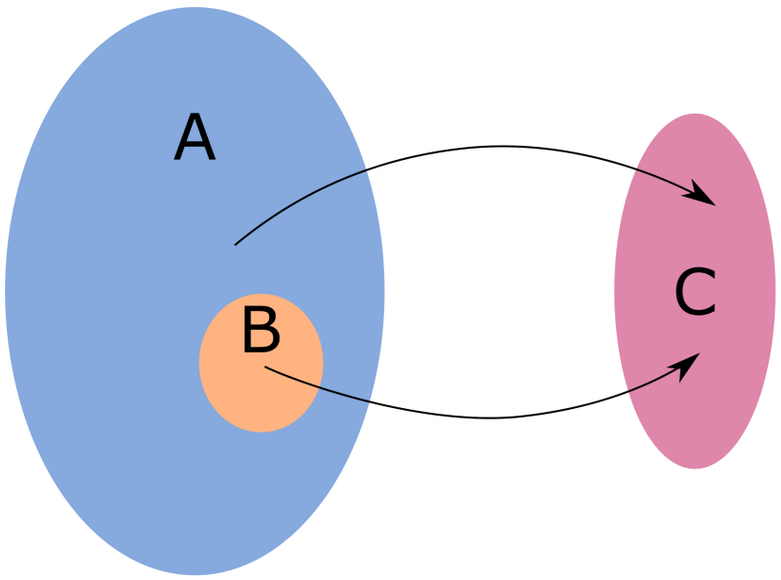

potential ambiguities
in the original network

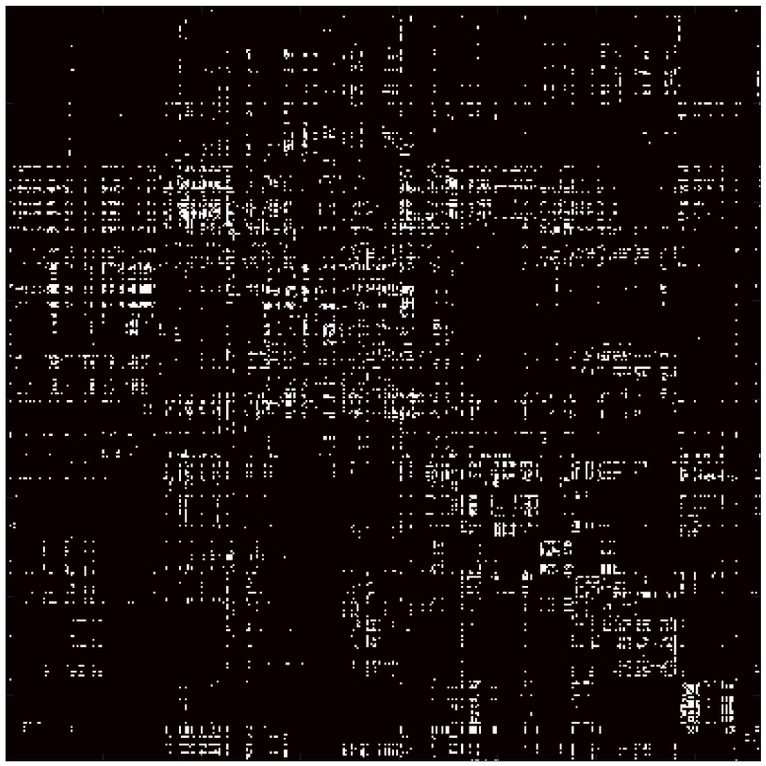

Modha & Singh network

#nodes : 383
#links : 6602

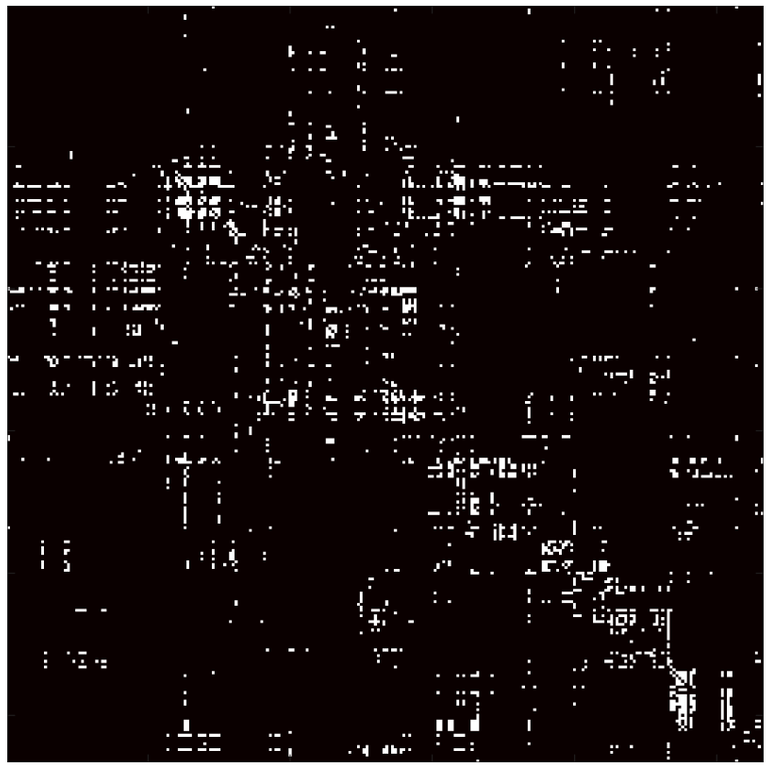

leaf node network

#nodes : 266
#links : 2602

- We only keep the nodes in the lowest hierarchical level, and the connections between them.
- The volume of the brain regions range from $\sim 2\,\mathrm{mm}^3$ (thalamic area PT#2) to $\sim 2000\,\mathrm{mm}^3$ (visual cortex area V1).
- Although we lose some connectivity information the macroscopic properties are very similar to the original network.

MACROSCOPIC OVERVIEW

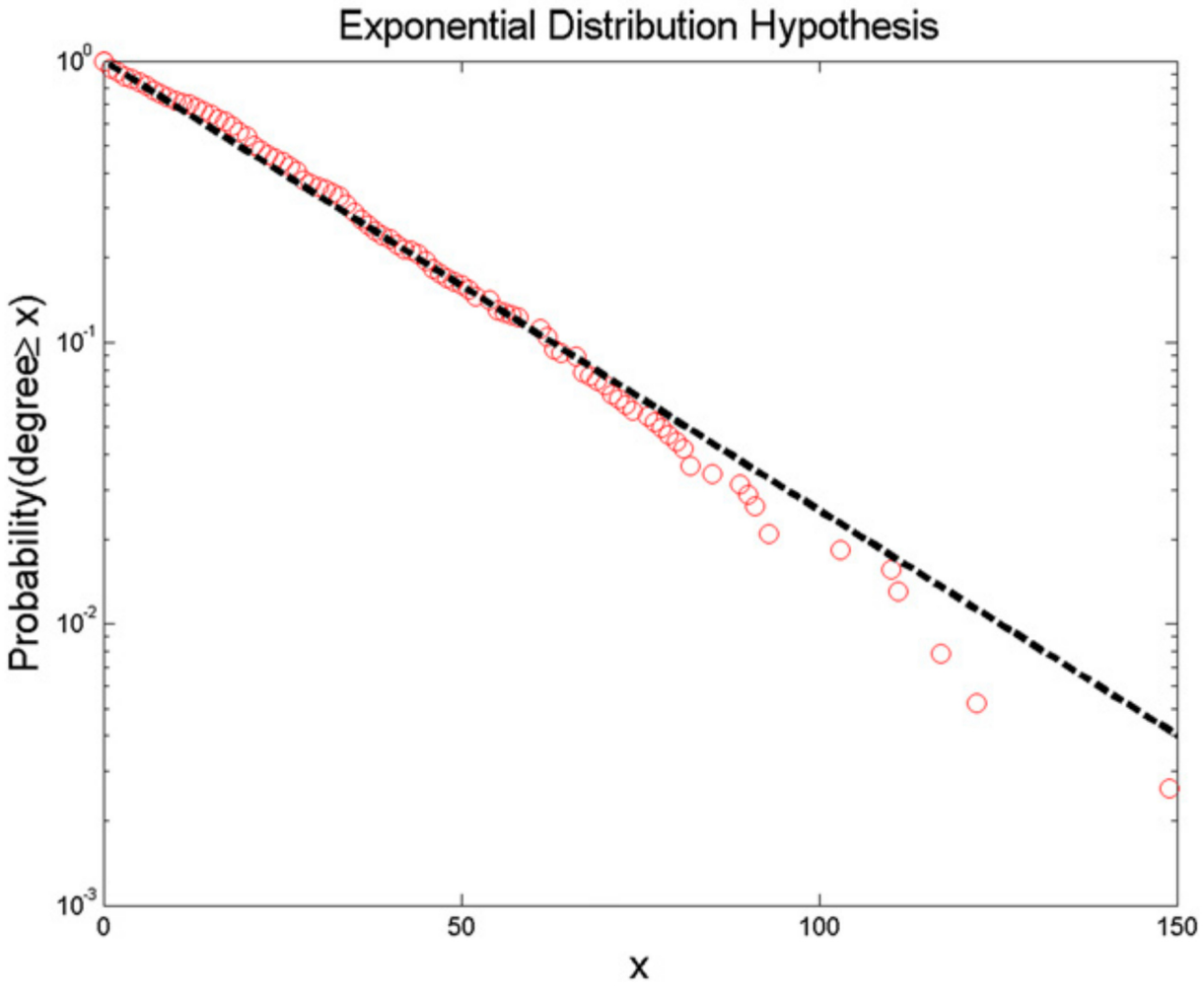

network of Modha & Singh (2010)
with directions removed

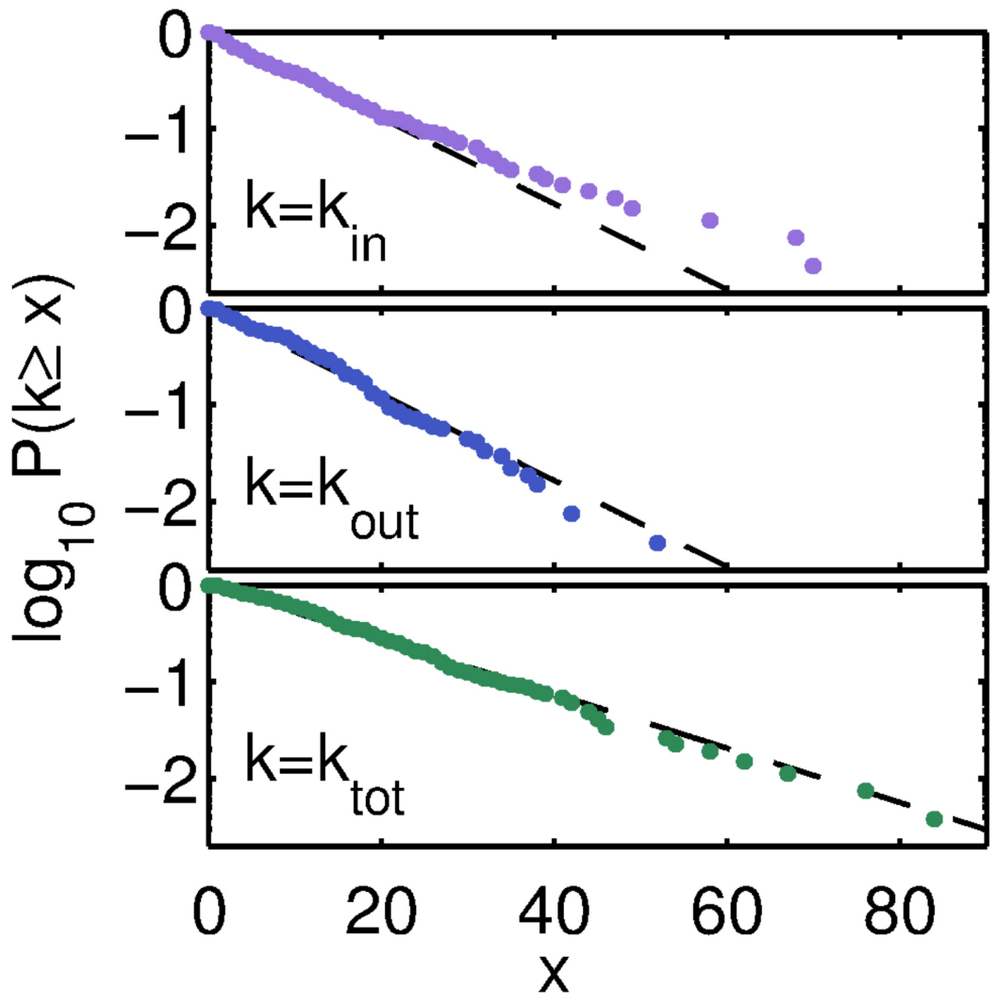

reduced network

images: DS Modha & R Singh, *PNAS* **107**(30), 13485 (2010); A Pathak, SN Menon, and S Sinha, *Phys. Rev. E* **106**, 054304 (2022).

PART 2: MODULARITY

image: Jacques Tati “PlayTime” (1967)

MEASURING MODULARITY

We can quantify the extent to which communities in a network are segregated as follows.

If g_i is the community that node i belongs to, then the *actual* number of edges between nodes of the same community is $\frac{1}{2}\sum_{ij} A_{ij}\,\delta_{g_i g_j}$. For a directed network, this is $\sum_{ij} A_{ij}\,\delta_{g_i g_j}$.

If the total number of links in the network is m, one can imagine $2m$ "stubs" (or m "in-stubs" and m "out-stubs" in a directed network).

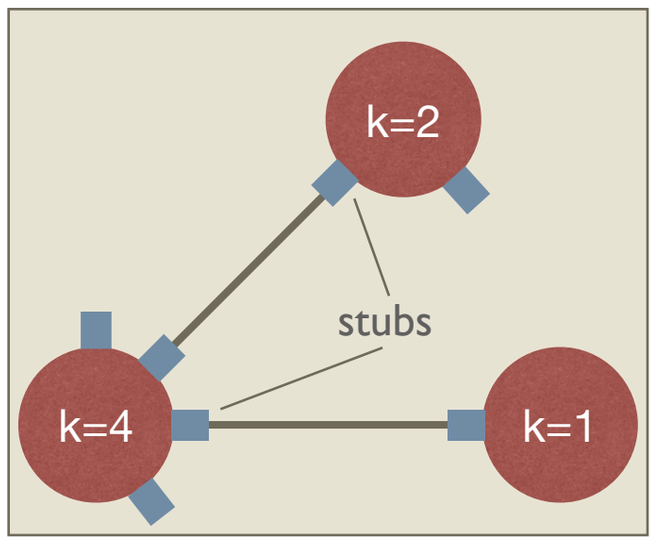

If all links were random (assuming a given number of stubs k_i per node i), then the *expected* number of links between stubs of nodes i and j is $k_i\,k_j/2m$ (or $k_i^{in}\,k_j^{out}/m$ in a directed network).

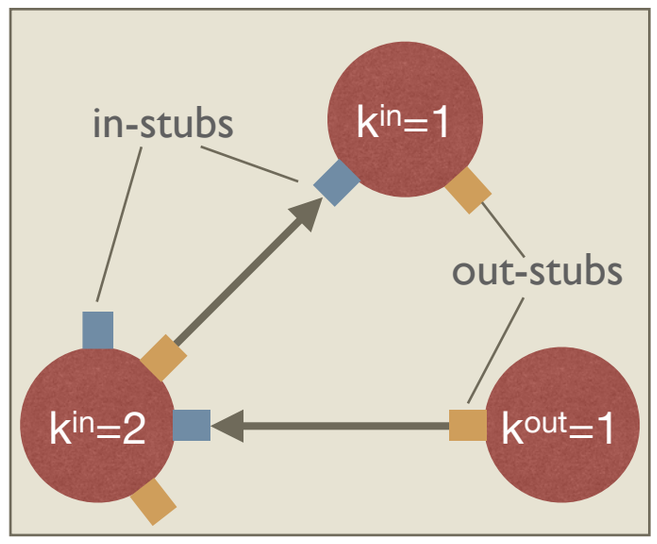

MEASURING MODULARITY

So the *expected* number of links between nodes belonging to the same community is $\frac{1}{2}\sum_{ij}\frac{k_i k_j}{2m}\delta_{g_i g_j}$, or $\sum_{ij}\frac{k_i^{in} k_j^{out}}{m}\delta_{g_i g_j}$ in a directed network.

Thus, the (normalized) difference between the *actual* and *expected* number of edges between nodes of the same group in an the two types of networks are given by:

$$Q_{undirected} = \frac{1}{2m}\sum_{ij}\left(A_{ij} - \frac{k_i k_j}{2m}\right)\delta_{g_i g_j}, \quad Q_{directed} = \frac{1}{m}\sum_{ij}\left(A_{ij} - \frac{k_i^{in} k_j^{out}}{m}\right)\delta_{g_i g_j}$$

Here, the quantity Q is referred to as the **modularity**. This gives us a measure of the excess number of links seen within groups than would be expected by chance.

DETERMINING THE MODULES

A number of approaches can be used to obtain the modular structure. One of the most common approaches involves modularity maximization.

For this, we assume that each node i is in one of two groups, and introduce the column vector $\mathbf{s}$ ($s_i = \pm 1$, depending on which group i belongs to). Then for an undirected network we have:

$$Q = \frac{1}{2m}\sum_{ij}\left(A_{ij} - \frac{k_i k_j}{2m}\right)\frac{s_i s_j + 1}{2} = \frac{1}{4m}\sum_{ij}\left(A_{ij} - \frac{k_i k_j}{2m}\right)s_i s_j = \frac{1}{4m}\sum_{ij} B_{ij} s_i s_j = \frac{1}{4m}\mathbf{s}^T\mathbf{B}\mathbf{s}$$

In the case of a directed network we use the fact that Q is equal to its own transpose, and so redefine it to be $(Q + Q^T)/2$, this yields:

$$Q = \frac{1}{2}\left(\frac{1}{2m}\mathbf{s}^T\mathbf{B}\mathbf{s} + \frac{1}{2m}\mathbf{s}^T\mathbf{B}^T\mathbf{s}\right) = \frac{1}{4m}\mathbf{s}^T(\mathbf{B} + \mathbf{B}^T)\mathbf{s}$$

* Newman, M. E. J., PNAS **103**, 8577 (2006); Leicht, E.A. & Newman, M. E. J., Phys. Rev. E **100**, 118703 (2008).

DETERMINING THE MODULES

Thus the problem can be reduced to the following :

Given the modularity matrix $\mathbf{B}$, find $\mathbf{s}$ such that Q is maximum.

A widely used method* known as the **Spectral Newman method** is based on the insight that the optimal $\mathbf{s}$ (were it not constrained to take values $s_i = \pm 1$) would be an eigenvector of $\mathbf{B}$. That is, we note that $\mathbf{B}\,\mathbf{s} = (4mQ)\,\mathbf{s}$.

So, finding the partition with the maximum Q involves finding the eigenvector of the largest eigenvalue of $\mathbf{B}$, and identifying the nodes with positive and negative values of $\mathbf{s}$.

This process is extended to (attempt to) subdivide each module into two until a given module can no longer be subdivided. Furthermore at each step, one applies the Kernighan-Lin algorithm, wherein every node in the subdivided modules are swapped if doing so would lead to an increase in Q.

* Newman, M. E. J., PNAS **103**, 8577 (2006); Leicht, E. A. & Newman, M. E. J., Phys. Rev. E **100**, 118703 (2008).

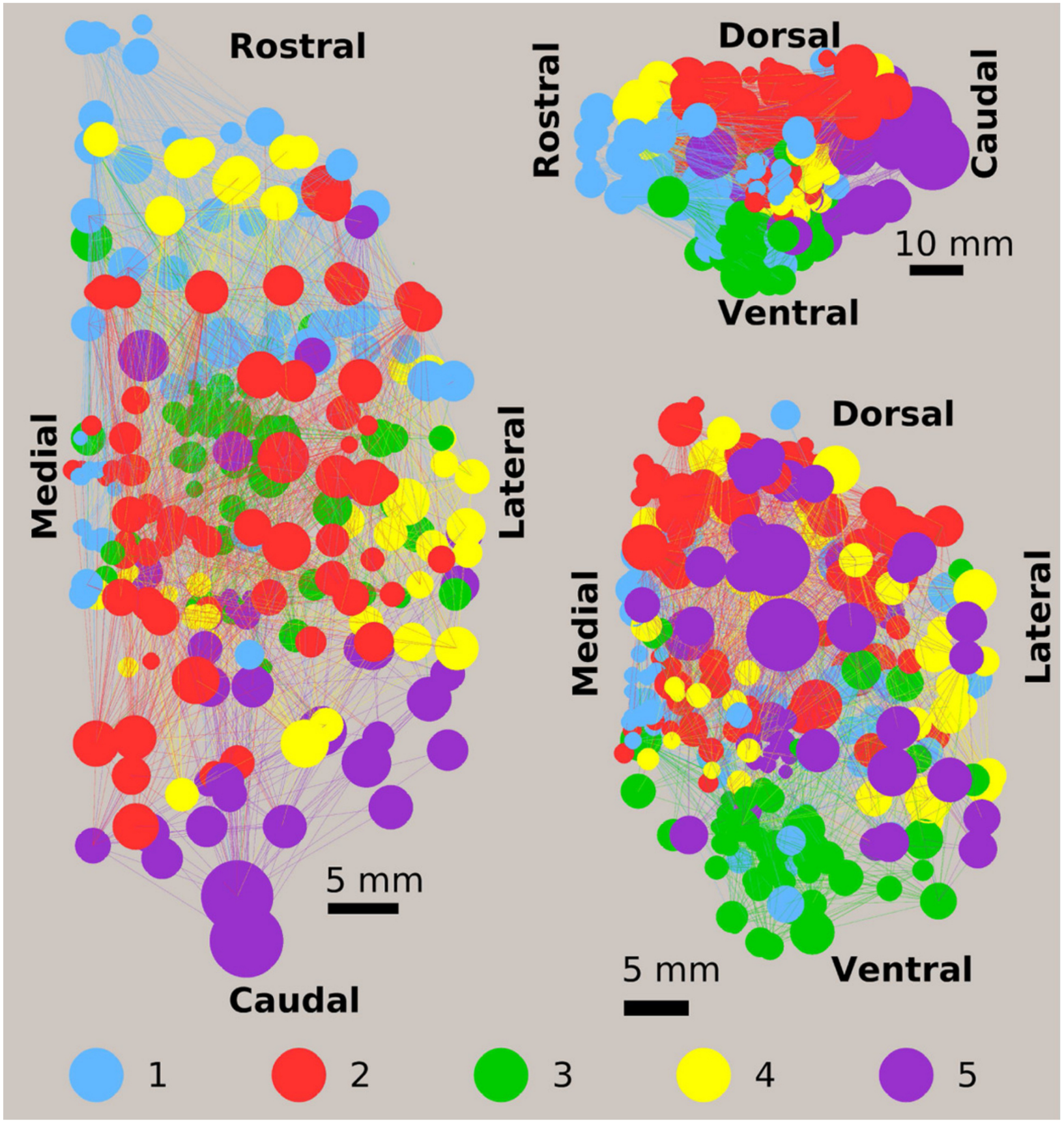

ProSt
Cs#2
OFap
Clc
PAa
10d
23a
23b
OFC
Cdc
AD#1
Cim
MDcd
32
14O
10v
Cif
AM#1
MDpm
Su#2
Sb
VAmc
24c
24a
12l
24b
TPdgd
6Vb
12o
6Va
Pu-r
Sl#2
12r
12m
13L
10o
11l
14r
11m
13M
10m
Iai
TPg
13a
Ial
Iam
Iapm
TPag
TPdgv
PrCO
MDfi
Gu
belt-s
EO

AV
Re
Pcn
CM#2
Csl
MI#1
Ret
Pul.o
MDpc
MDmf
X
VPS
VPl
VPM
VPLo
VPLc
VLm
VLps
VLo
VLc
VApc
VAdc
belt-sm
ProM#2
47/12
9/46v
45B
F5
4c
F4
44
F7
F2
SMAr
SMAc
M2-HL
M2-FL
F6
M1-FL
MI-of
MI-body
M1-HL
1#1
2#1
3b
3a
SII-f
PR#4
PFop
PP
PGop
PFG#1
PF#1
AIP
MIP
PEm
5-Foot
PEc#1
PGm
31
PECg
24d
23c
TSA
Ri#1
IPro
V6A
Pu-c
Clau
MTp
8Ad

PT#2
6b-beta
4b
4a
Sub.Th
ELc
CMA#2
Hyp
ER#1
29d
29a-c
DG
Cd-t
SN
CA3
I#2
ECL
EI
PaS
36p
EC#2
PrS
28m
ME#1
COa
TEa#3
TFM
Pi#1
TFL
Pros.
35
MB
AITv
CA1
TH
36c
ABmg
Bla
Abpc
36r
CE#1
Bi
PAC2
A
AHA
Bvl
Lv
ABvm
ABd
ABv
Ldi
Lvl
COp
NLOT
Ld#2
Idg
Ig#1
25
CITd
ELr

MG
SG
Li
PMm
PMl
PLd
L9
46v
46d
PS
46f
46vr
46dr
9/46d
8B
PG#1
Opt
CML
30
ProK
paAc
L#1
CL#4
ST3
Tpt
TPOc
TPOi
TPOr
TAa
PGa
AL#4
A1
STPg
ST2
ST1
M9
D9
MDdc
Pf#2

LGN
PIl-s
PIp
PIm
PIl
PIc
PLa#1
PLvl
PLvm
45A
8Ac
LIPe
LIPi
VIP
PIP#1
CITv
TEm
PITd
PITv
IPa
MT
FST
MSTp
MSTd
V3A
V3d
V3v
V4t
DLr
DLc
V4v
VPP
DI#1
V6
DP
VOT
V1
V2
Cd-g
MB#2
LD#1
GPe

image: A Pathak, SN Menon, and S Sinha, *Phys. Rev. E* **106**, 054304 (2022).

Basal Ganglia

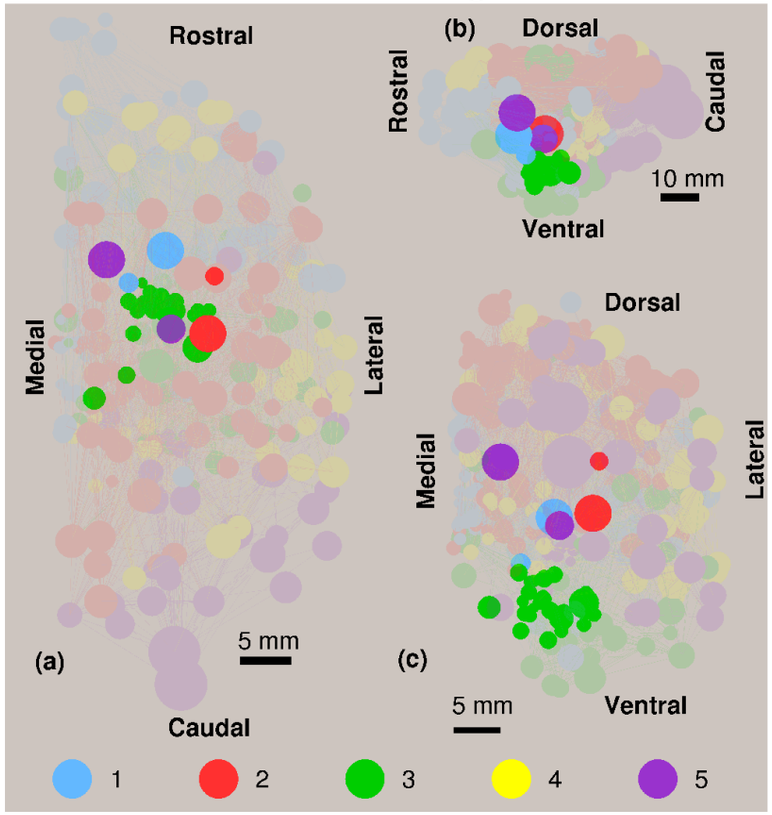

Occipital Lobe

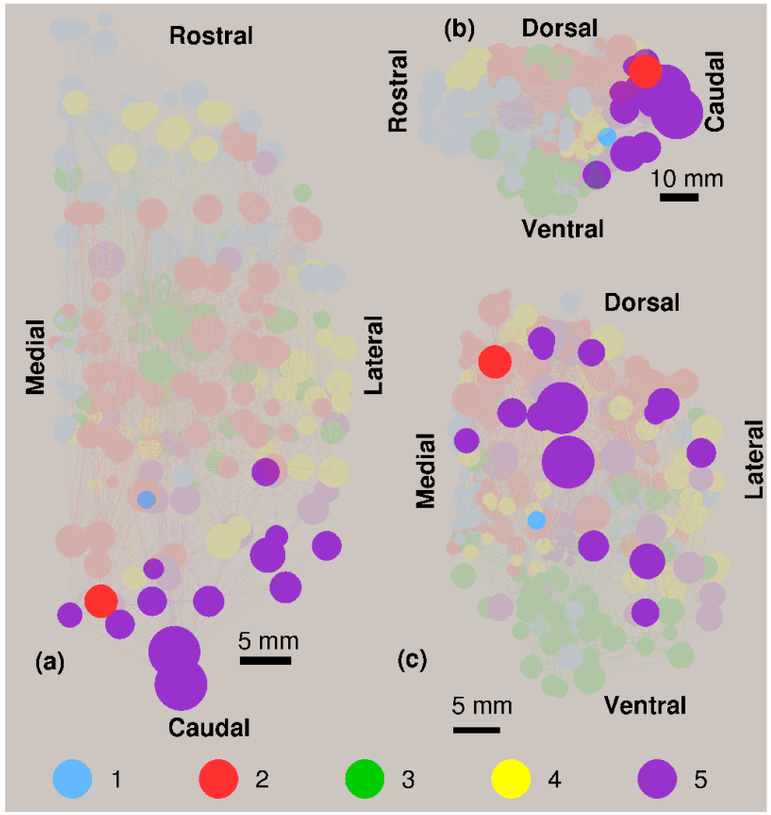

Temporal Lobe

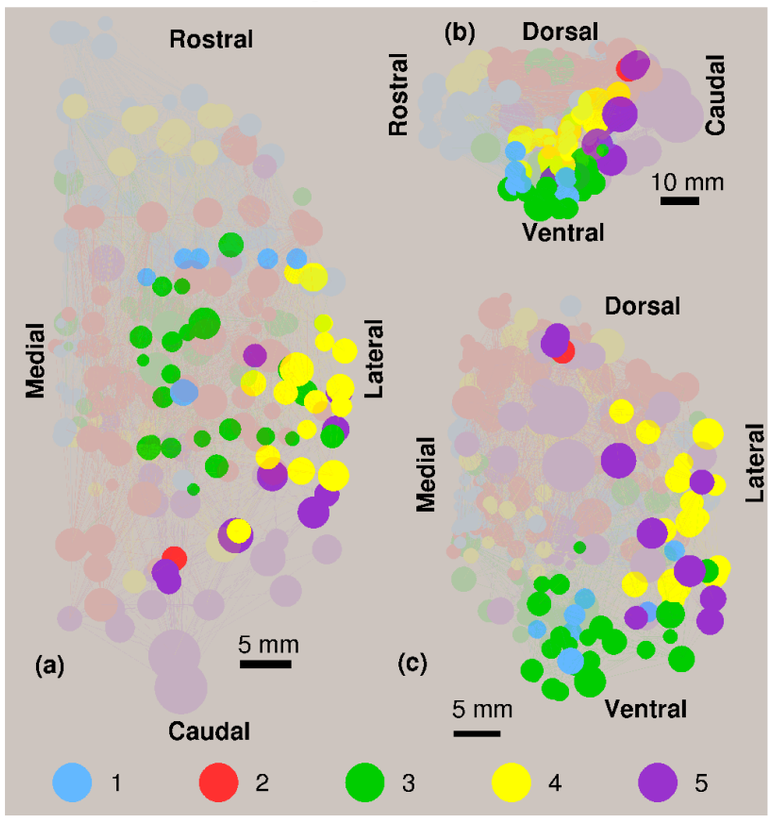

Insula

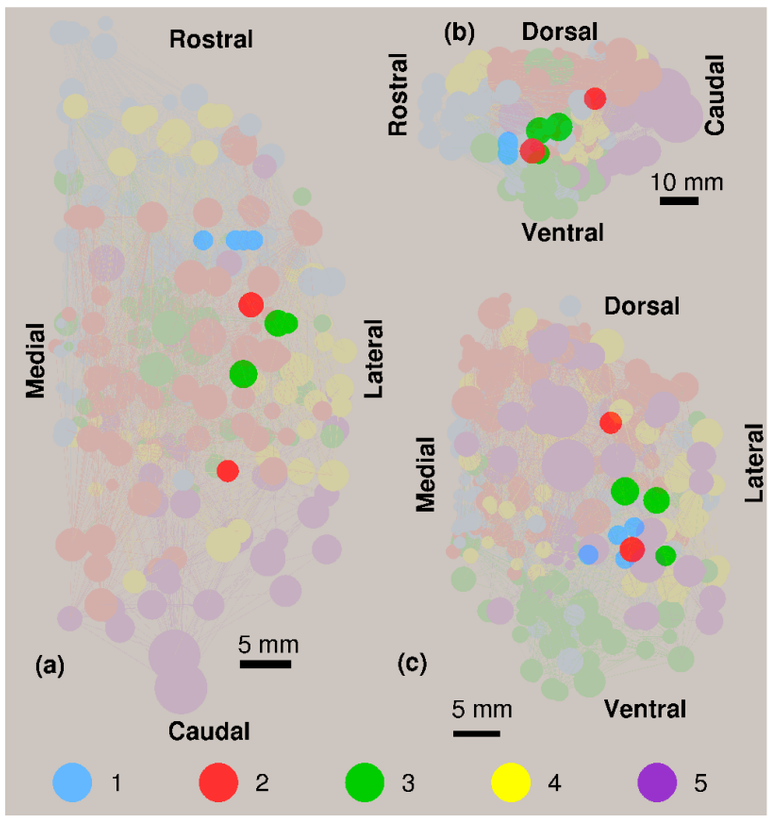

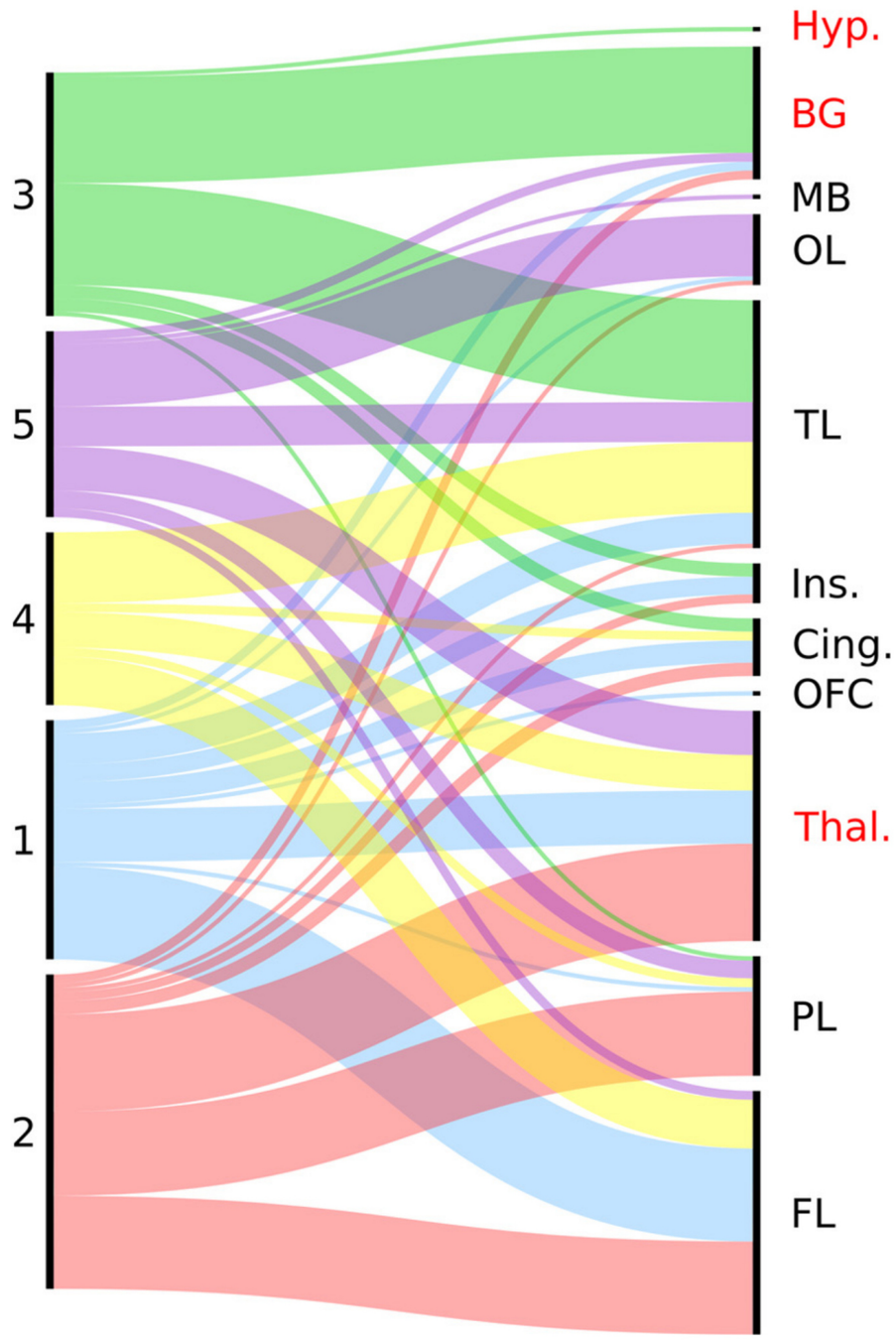

image: A Pathak, SN Menon, and S Sinha, *Phys. Rev. E* **106**, 054304 (2022).

Cingulate

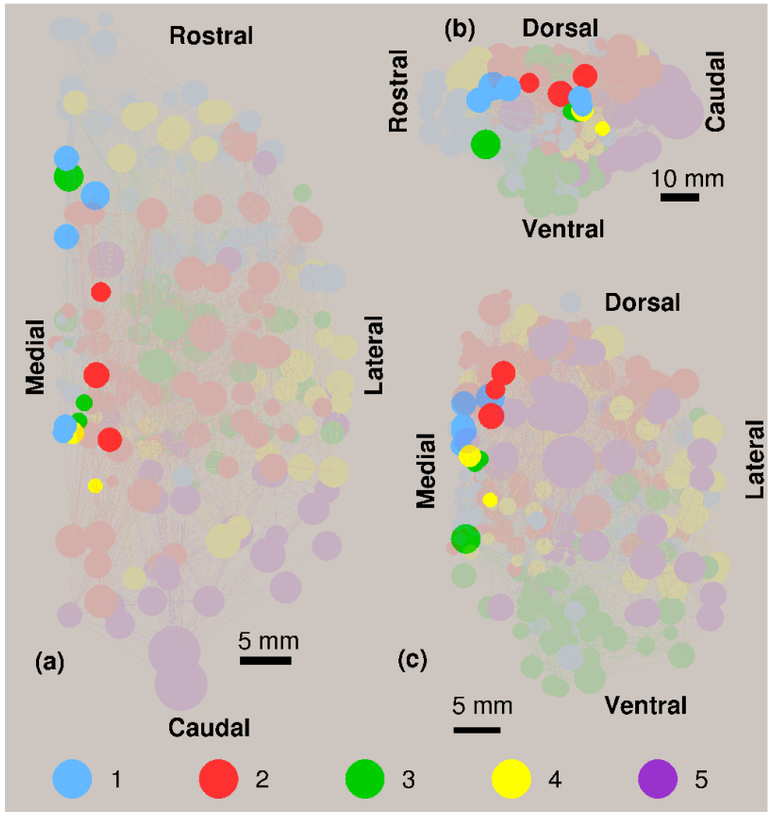

Thalamus

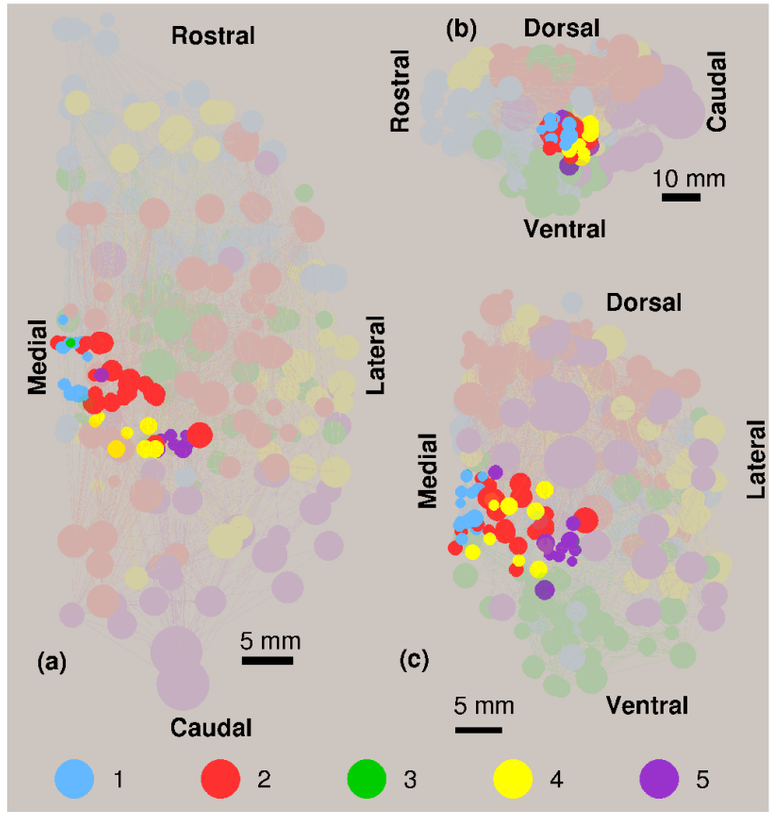

Parietal Lobe

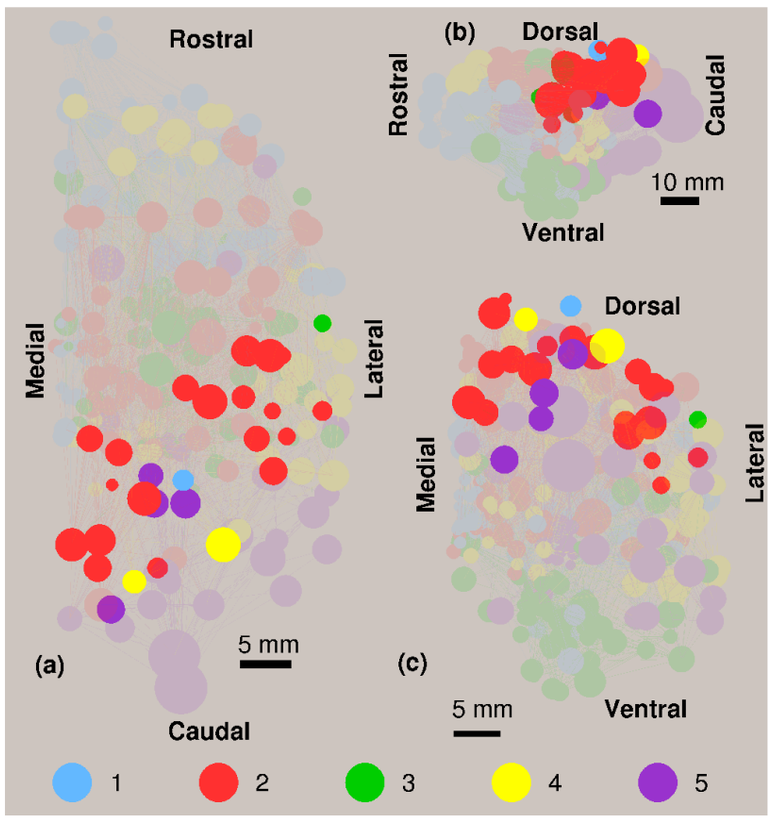

Frontal Lobe

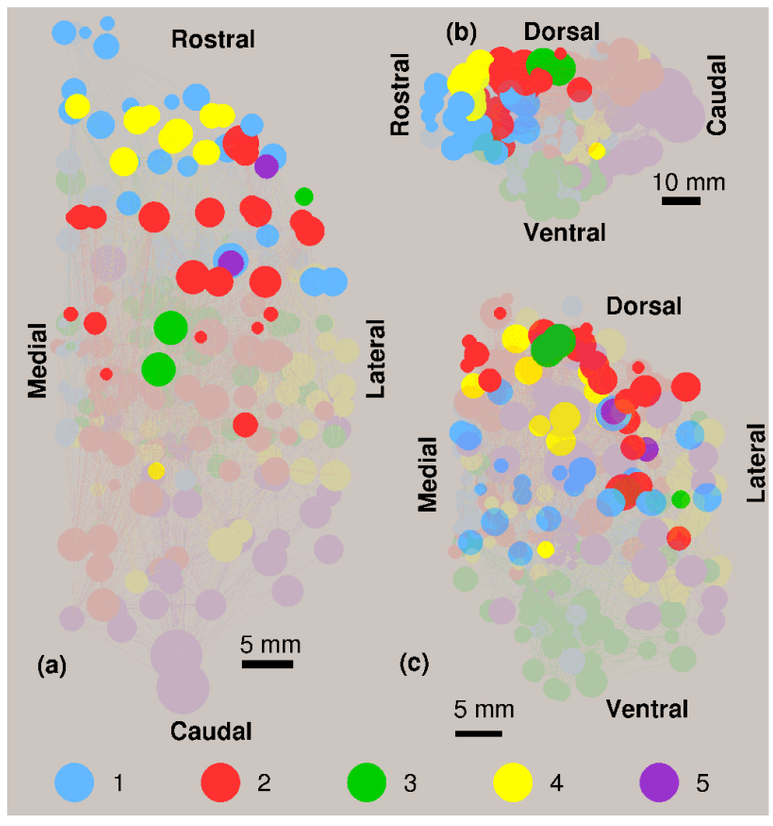

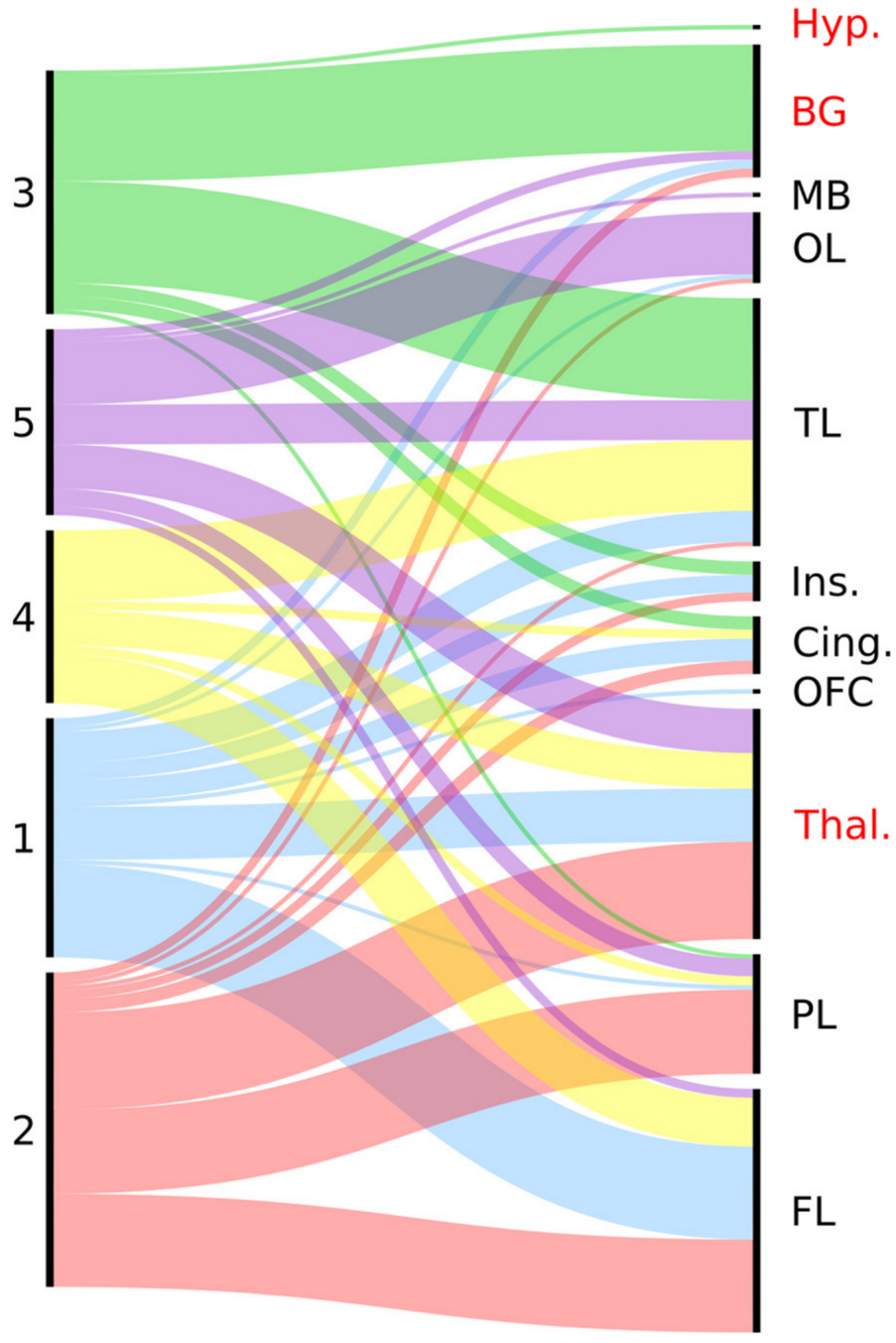

image: A Pathak, SN Menon, and S Sinha, *Phys. Rev. E* **106**, 054304 (2022).

There exists a general organisational scheme, with each of the principal **sensory modalities** localized in specific modules:

- module #1: olfactory/gustatory (e.g. olfactory complex)
- module #2: somatosensory (e.g. Area 6, Ventolateral Nucleii of Thalamus)
- module #4: auditory (e.g. superior temporal gyrus)
- module #5: visual (e.g. Visual anterior cortex, nucleus pulvinar thalami)

Module #3 does not include any primary or secondary sensory areas but does contain the amygdala which regulates emotional responses and fear conditioning.

Module 5						
Lobe/nuclei	Subdivision	Frac.	$\langle PC \rangle$	$\langle z \rangle$	Specific areas	Known function
Frontal lobe	PFC	2/36	0.28	-0.30	45A, 8Ac	saccadic guidance (frontal eye field) [113]
Temporal lobe	TE	4/7	0.47	0.03	CITv, PITd, PITv,TEm	ventral visual pathway [76,77]
	STS	5/11	0.44	1.28	MT, MST, FST	dorsal visual pathway [76,77]
Parietal lobe	PCip	4/6	0.43	0.06	LIP, VIP, PIP	visual attention [92,93]
Occipital lobe	VAC	12/13	0.11	-0.23	V3A, V3B, V6	visual cortex [61]
	V1	1/1	0.25	1.28		primary visual cortex [61]
	V2	1/1	0.39	3.15		secondary visual cortex [61]
Thalamus	AN	1/4	0.69	-0.51		
	GN	1/2	0.28	-0.59	LGN	visual information relay [61]
	Pul#1	8/12	0.06	-0.70		visual processing [127]
Basal Ganglia	Gpe	1/1	0.67	-0.84		
	STR	1/4	0.65	-0.10	Cd_g	reinforcement learning [110]
Mid brain	MB	1/1	0.30	-0.19		

image: A Pathak, SN Menon, and S Sinha, *Phys. Rev. E* **106**, 054304 (2022).

WHAT IS THE MOST "OPTIMAL" PARTITION?

- How can we be sure that the modular partitions are not sensitively dependent on the method used to find them?
- Using a stochastic simulated annealing technique* we perform 10^3 realizations using a "cooling schedule" and display a landscape of the resulting Q values.
- The procedure involves starting with a random partition and at each step we either
  - move a random node to a different module
  - merge two randomly chosen modules, or
  - split a random module into two, to minimize connections between them.
- If the new partition leads to a change ΔQ, it is accepted with probability $\exp(-|\Delta Q|/T)$ if $\Delta Q < 0$ and $p = 1$ otherwise.
- We see that at best there exist partitions that are *very close* to $Q_{emp} = 0.485$. Of the 10^3 partitions 291 of them have a modularity that is within $3\,\%$ of Q_{emp}.

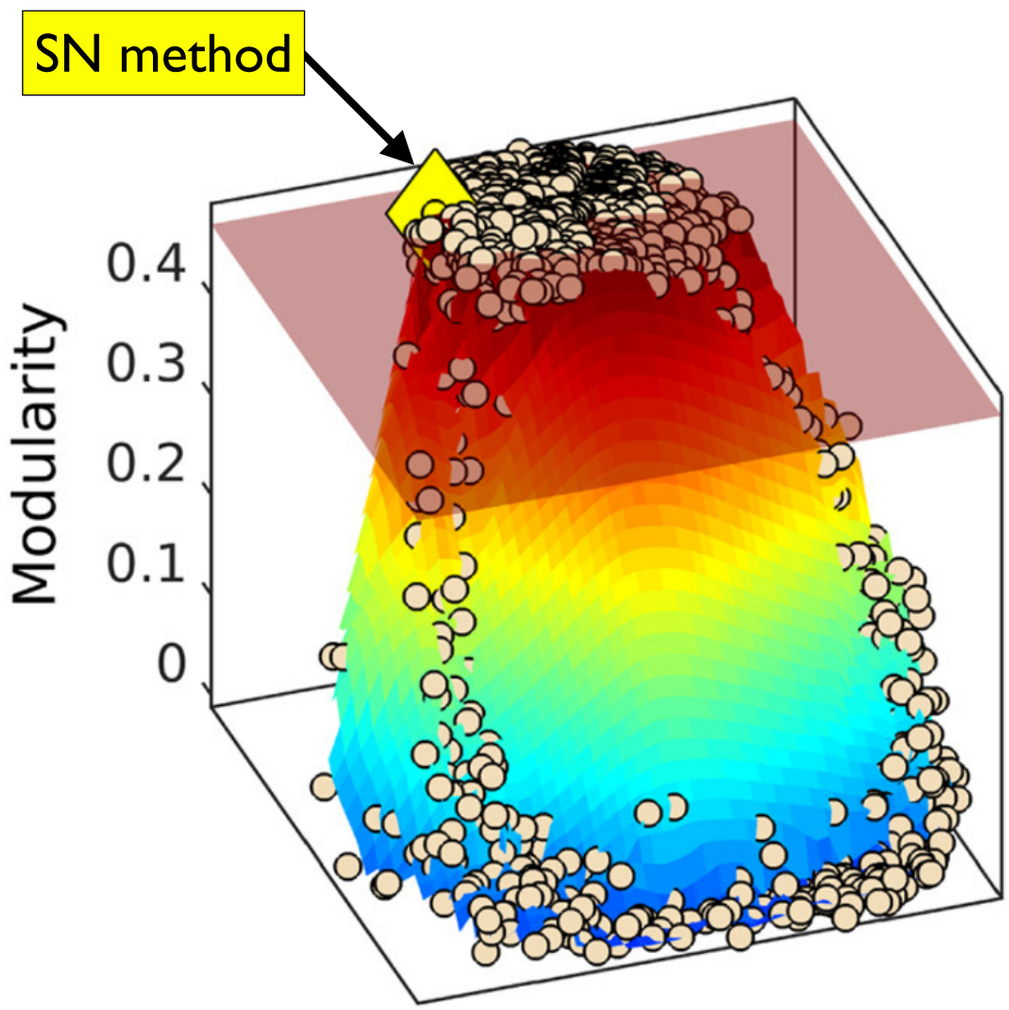

image: A Pathak, SN Menon, and S Sinha, *Phys. Rev. E* **106**, 054304 (2022).

* BH Good, Y.A de Montjoye & A Clauset, *Phys. Rev. E* **81**, 046106 (2010); https://aaronclauset.github.io/modularity/

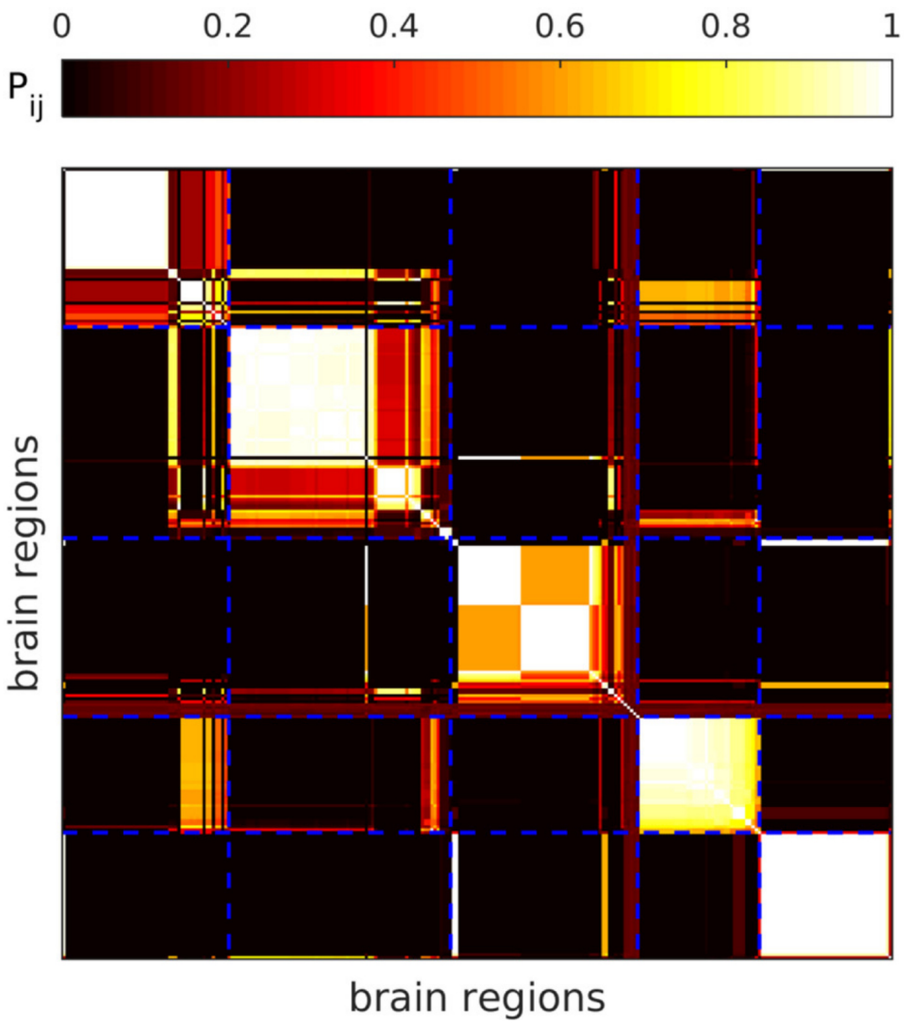

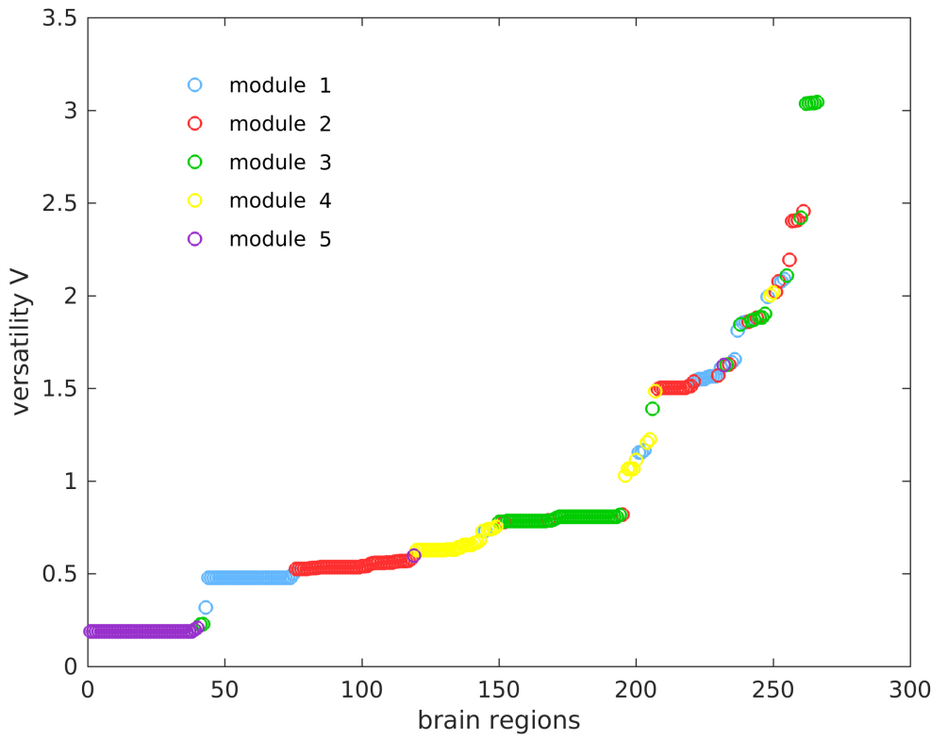

- Around $70\,\%$ of brain areas in these 291 partitions always occur in the same module as in the SN decomposition.
- On the right we display a consensus matrix $\mathbf{P}$, where each P_{ij} is the probability that a given pair of nodes (i, j) are found in the same module.
- We see that module 5 is almost completely consistent across all partitions.
- This observed consistency of $70\,\%$ of nodes can be most clearly seen by considering the versatility V, defined as

$$V_i = \frac{\Sigma_j \sin(\pi P_{ij})}{\Sigma_j P_{ij}}$$

- We see that V_i is highest when $P_{ij} = 0.5$ for all $j \neq i$, and is lowest when all P_{ij} values are either 0 or 1.

images: A Pathak, SN Menon, and S Sinha, *Phys. Rev. E* **106**, 054304 (2022).

PART 3: “FUNCTIONAL CARTOGRAPHY”

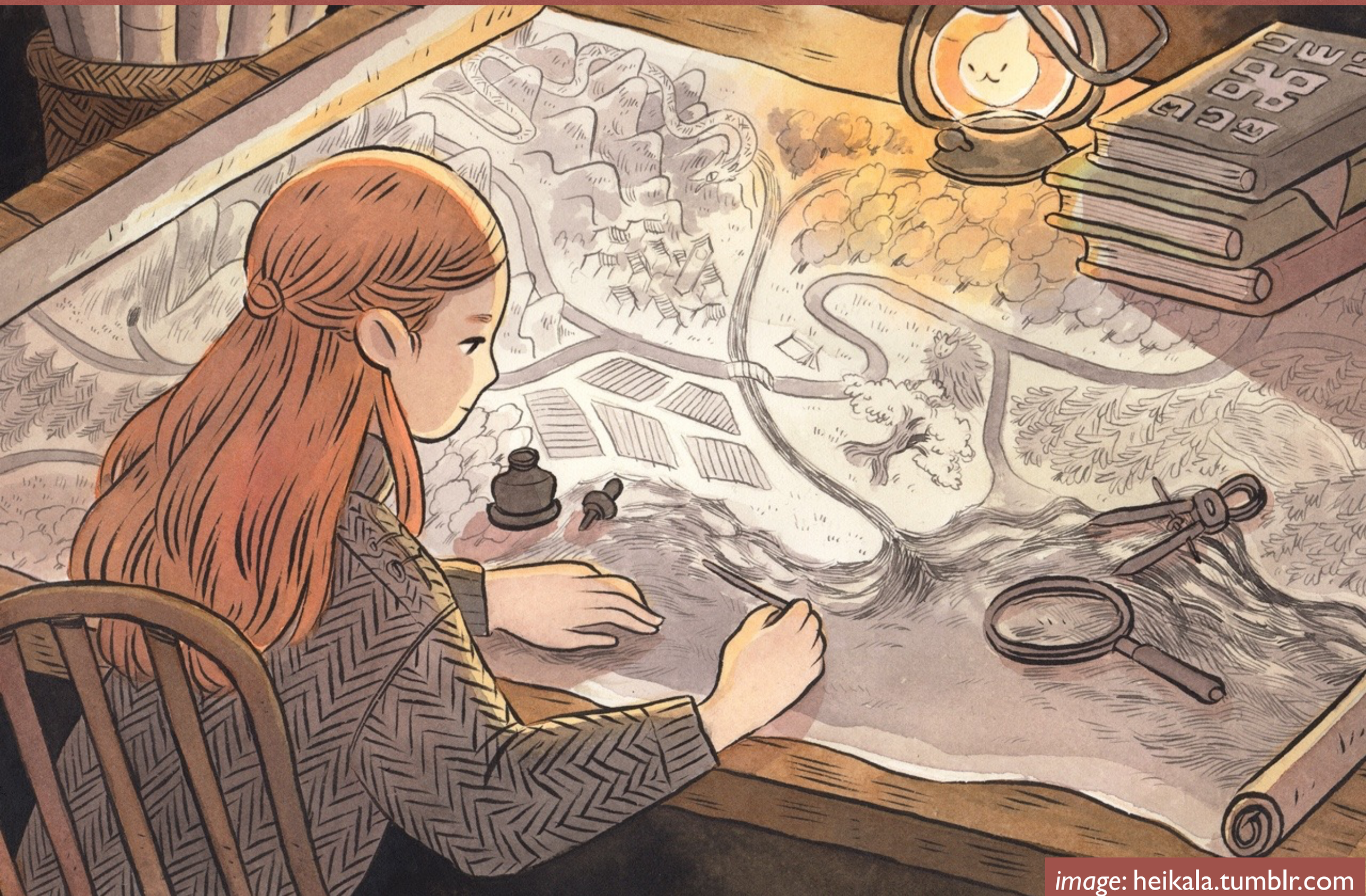

image: heikala.tumblr.com

CONNECTIONS WITHIN AND ACROSS MODULES

To identify areas that have significantly more (or less) connections within their own module, we compute the within-module degree z-score of each node:

$$z_i = \frac{k^i_{c_i} - \langle k^j_{c_i} \rangle_{j \in c_i}}{\sqrt{\langle (k^j_{c_i})^2 \rangle_{j \in c_i} - \langle k^j_{c_i} \rangle^2_{j \in c_i}}}$$

where $k^i_{c_i}$ are the number of links between area i and all other areas belonging to its module c_i .

To distinguish between brain areas in terms of their inter-modular connectivity, we calculate the participation coefficient:

$$\Pi^c_i = 1 - \sum_{c=1}^{m} \left(\frac{k^i_c}{k^i} \right)^2$$

where $k^i_{c_i}$ are the number of links between area i and a specified module c, and k^i is the degree of area i. If an area only has connections within its module then $\Pi^c_i = 0$.

FUNCTIONAL ROLES OF NODES

Using these two measures, a classification was proposed* with seven heuristically defined roles:

R1: ultra-peripheral nonhubs

R2: peripheral nonhubs

R3: connector nonhubs

R4: kinless nonhubs

R5: provincial hubs

R6: connector hubs

R7: global/kinless hubs

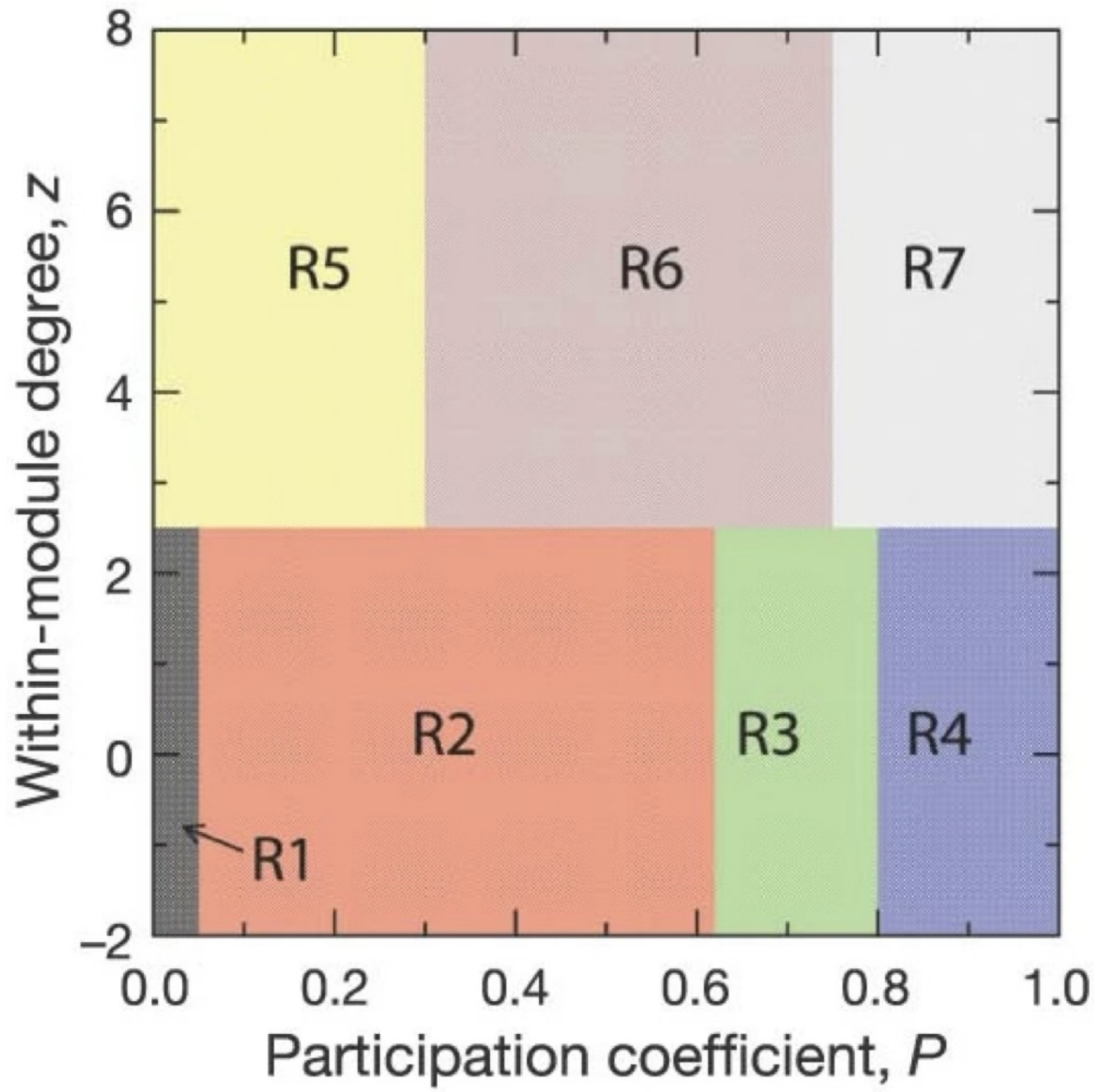

* R Guimera & LAN Amaral, *Nature*, **433**, 895 (2005).

FUNCTIONAL CLASSIFICATION OF MACAQUE BRAIN

Following Pan et al* we set the z-score threshold as 0.7 and use the same participation coefficient thresholds as in Guimera & Amaral.

We see areas in each module have a similar distribution across R1–R3 and R5–R6 (except module 4 which does not appear in R5).

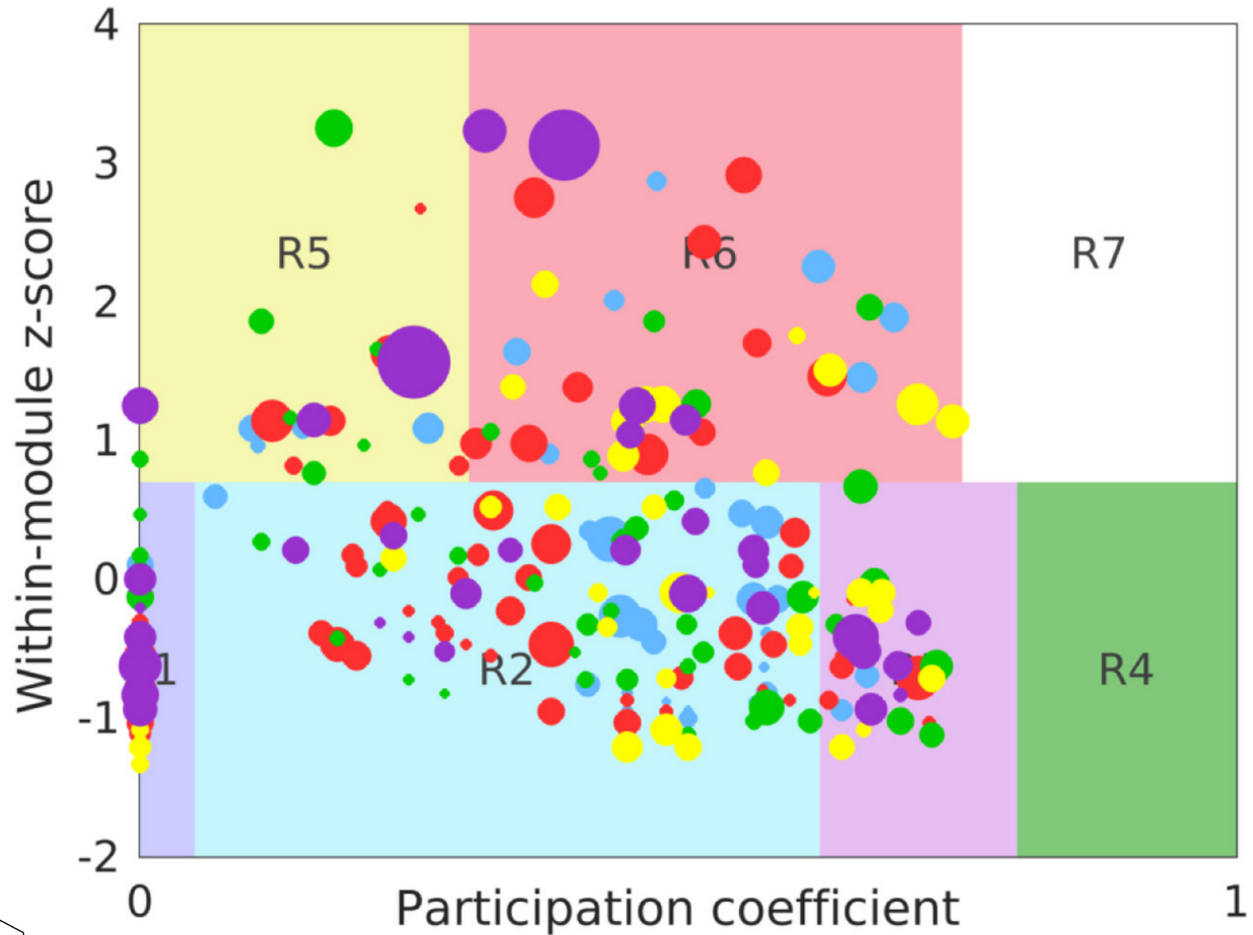

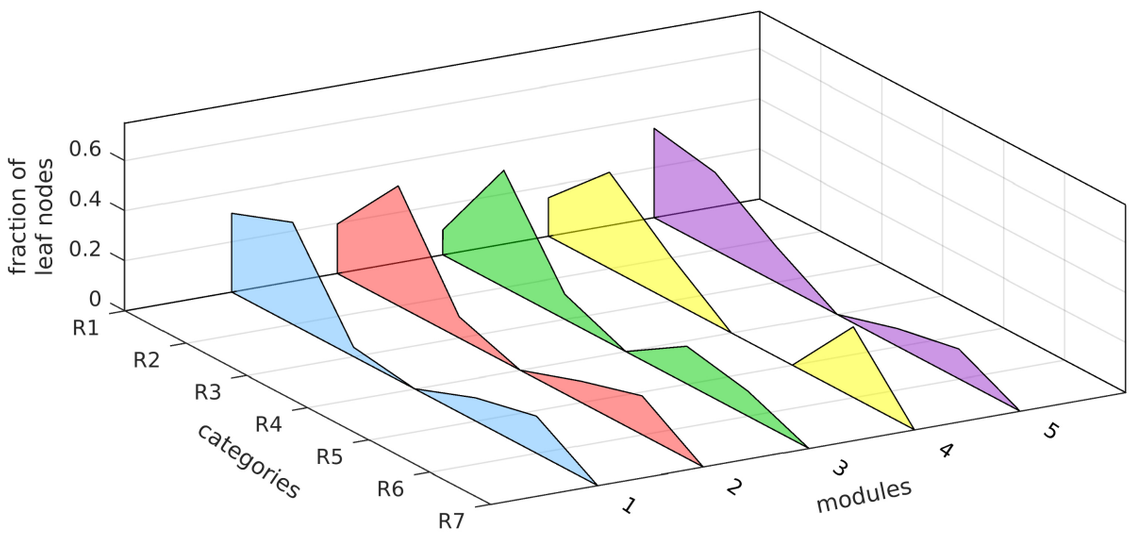

images: A Pathak, SN Menon, and S Sinha, *Phys. Rev. E* **106**, 054304 (2022).

* RK Pan, N Chatterjee & S Sinha, *PLOS ONE* **5**, e9240 (2010).

DISTRIBUTION OF MACAQUE BRAIN REGION ACROSS R1-R7 CATEGORIES

If we consider the entire brain, as well as the areas belonging to regions in the second hierarchical level, we see a similar "fingerprint" in terms of distributions across the functional categories.

The only regions that deviate are the Striatum and Thalamus that are virtually devoid of hubs (R5-R7), indicating relative homogeneity in the intramodular connectivity,

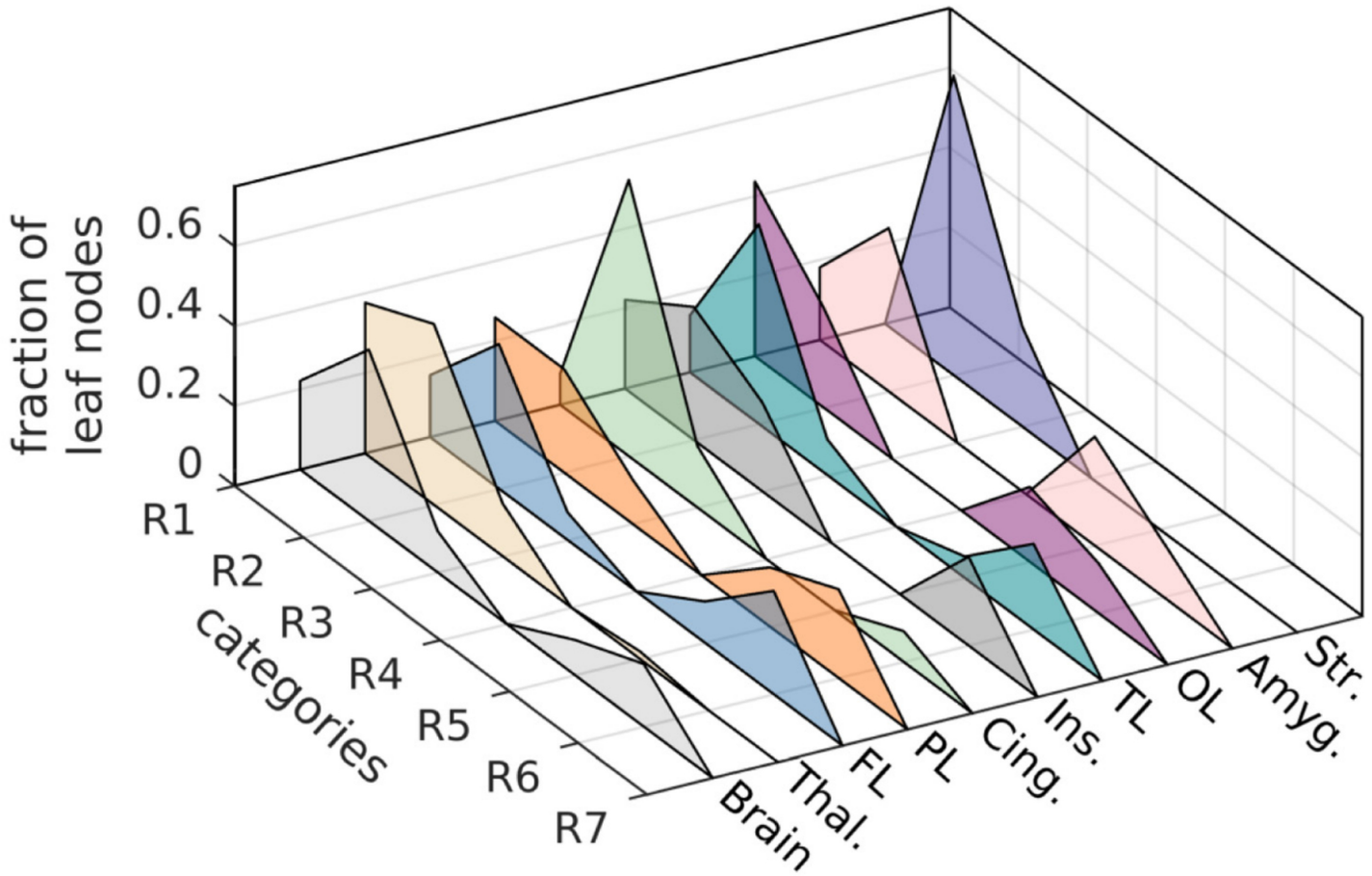

image: A Pathak, SN Menon, and S Sinha, *Phys. Rev. E* **106**, 054304 (2022).

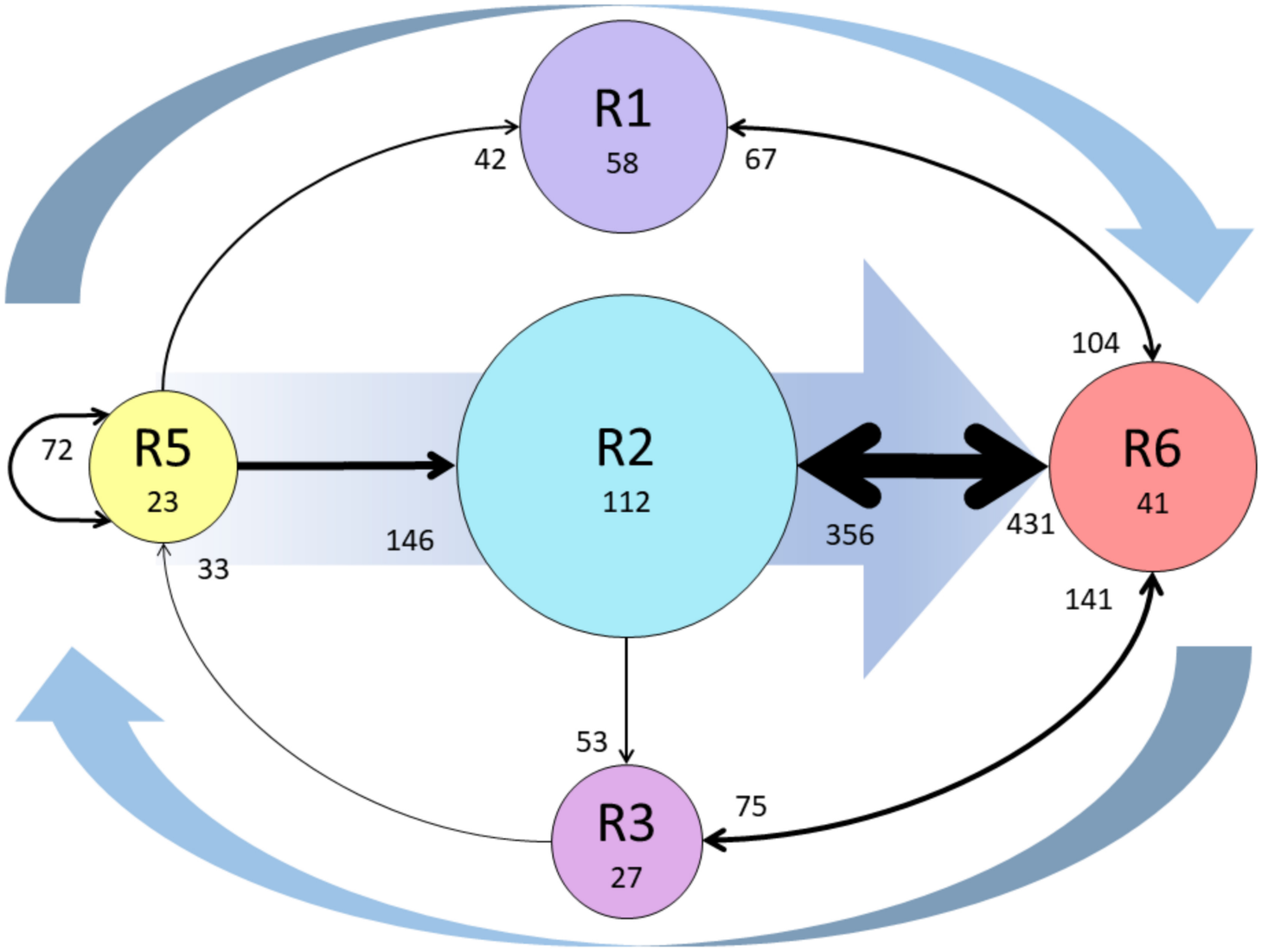

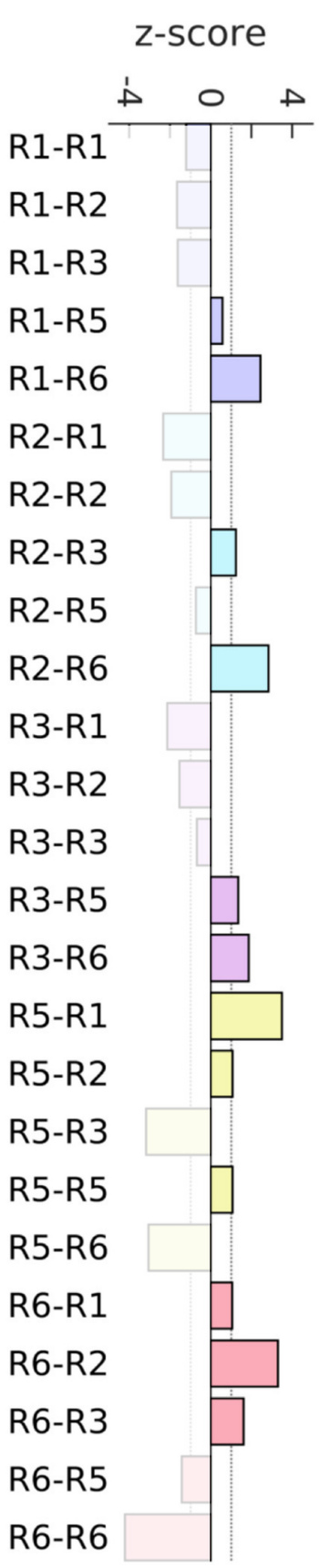

We can compute the z-score of connections between nodes of each functional category with respect to that obtained for networks in a DM (degree & module preserved) random ensemble.

Large positive or negative values imply connection types that are more or less likely than expected.

Considering the statistically significant connections suggests a mesoscopic pattern of information flow along the network.

images: A Pathak, SN Menon, and S Sinha, *Phys. Rev. E* **106**, 054304 (2022).

ENHANCED SPREAD OF INFORMATION

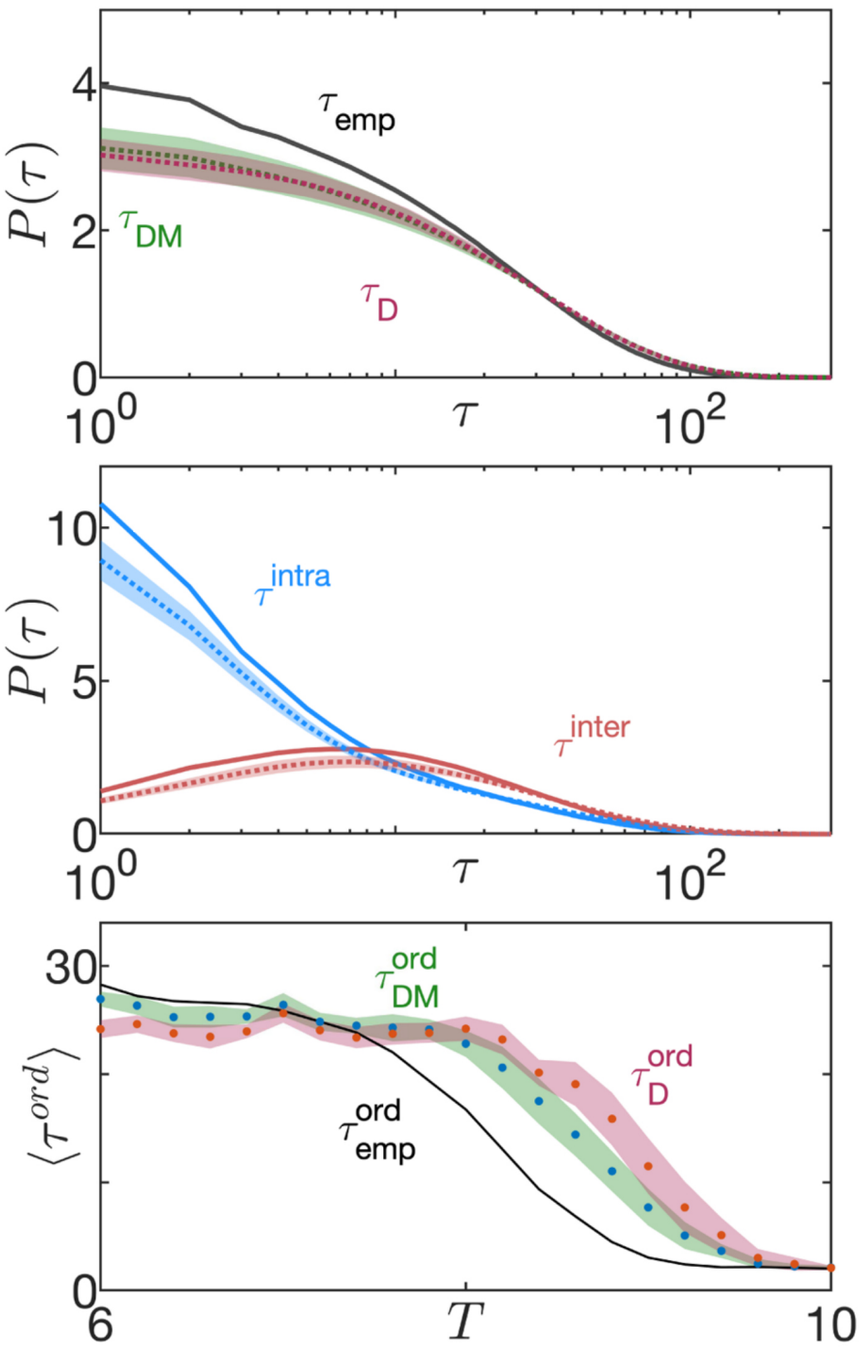

We measure the first passage time τ that a random walker placed at a given node i reaches a node j.

Comparing the probability $P(\tau)$ for the empirical network (τ_{emp}) with that of the degree-preserved (τ_D) and degree and module preserved (τ_{DM}) random networks, we see that the empirical network yields the lowest τ values.

A similar behaviour is observed when considering random walkers that remain within a module (τ^{intra}) or those that search for a node in a different module (τ^{inter}).

We also find that empirical network shows the shortest average time taken to reach an ordered state $\langle \tau^{ord} \rangle$ in the case where Ising spins are placed at each node.

Thus, the specific connectivity of the macaque brain allows for enhanced communication between brain regions.

image: A Pathak, SN Menon, and S Sinha, *Phys. Rev. E* **106**, 054304 (2022).

ENHANCED SPREAD OF INFORMATION

We compute the z-score of the τ values of the empirical network compared with the randomised ensembles.

We obtain this for the full network as well as the cases where the sources are in R1-R7.

In all cases, there is a statistically significant shift towards lower τ values.

The shift is more apparent for inter-module walkers (except for those that start in R3).

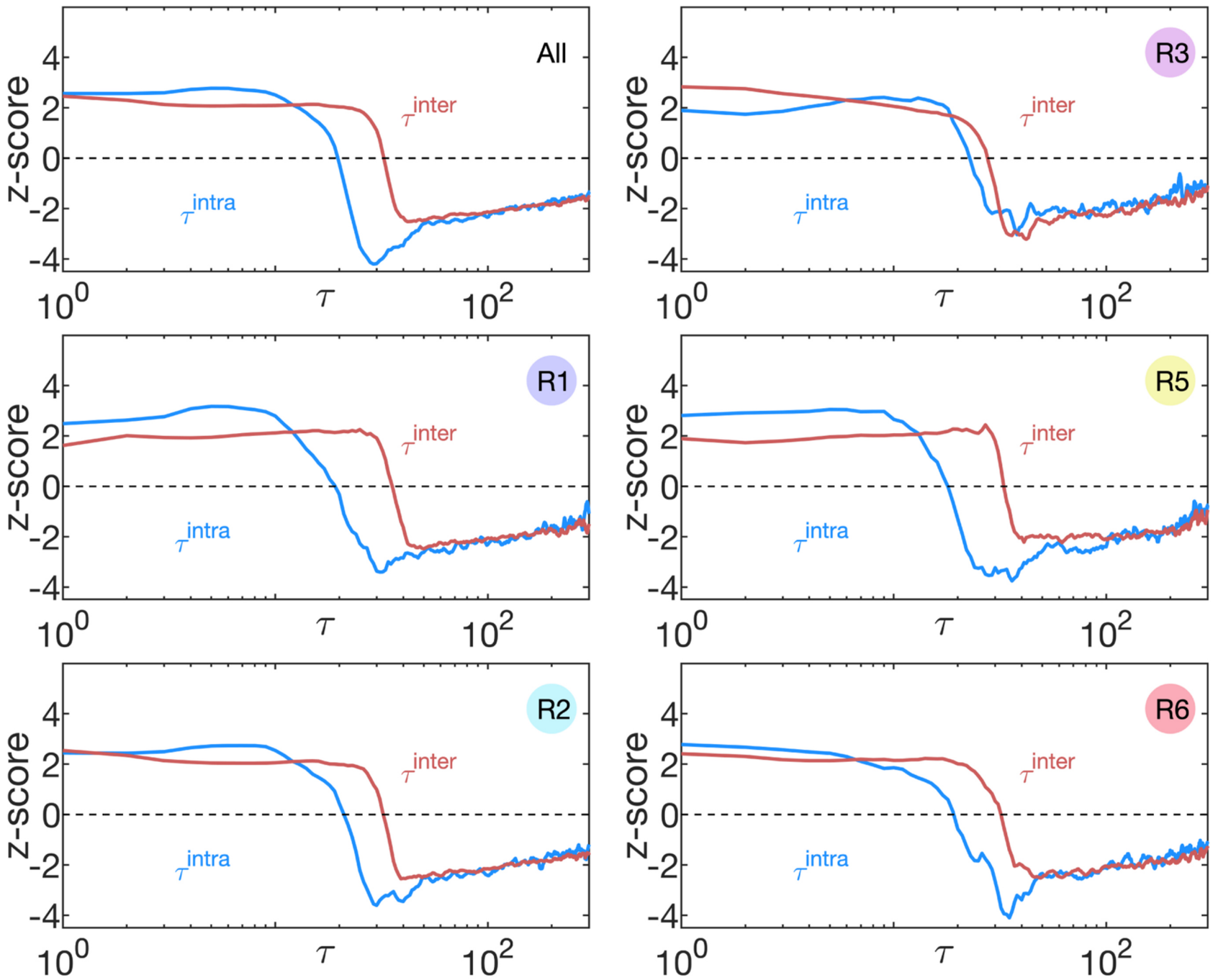

image: A Pathak, SN Menon, and S Sinha, *Phys. Rev. E* **106**, 054304 (2022).

PART 4: DO THE POSITIONS MATTER?

image: Ingmar Bergman, "Det sjunde inseglet" (1957)

SPATIAL INFORMATION OF MACAQUE BRAIN REGIONS

	A	B	C	D	E	F	G	H	I
1				Stereotactic coordinates (mm)					
2	**Node**	**Area**	**Name**	**x**	**y**	**z**	**Volume (mm^3)**	**Module**	**Categories**
3	1	Hyp	Hypthalamus	1.09	-6.75	9.78	100	3	R3
4	2	LD#1	Laterodorsal nucleus	4.30	-12.15	20.80	12	5	R3
5	3	AV	Nucleus anterior ventralis thalami	2.83	-9.00	20.15	9	2	R3
6	4	AM#1	Nucleus anterior medialis thalami	1.76	-9.00	18.62	4	1	R2
7	5	AD#1	Nucleus anterior dorsalis thalami	2.93	-10.35	20.37	2	1	R2
8	6	Re	Nucleus reuniens thalami	0.64	-9.00	14.50	7	2	R2
9	7	PT#2	Nucleus parataenialis thalami	1.30	-9.00	20.60	2	3	-
10	8	PAa	Nucleus paraventricularis thalami, pars anterior	0.55	-6.75	17.53	2	1	R2
11	9	Clc	Nucleus centralis latocellularis thalami	0.44	-9.45	15.13	5	1	R2
12	10	Cim	Nucleus centralis intermedialis thalami	0.55	-13.05	15.57	3	1	R1
13	11	Cif	Nucleus centralis inferior thalami	0.70	-13.05	13.70	5	1	R2
14	12	Cdc	Nucleus centralis densocellularis thalami	0.66	-9.45	18.73	5	1	R2
15	13	MG	Corpus geniculatum mediale	8.90	-17.10	10.44	22	4	R1
16	14	LGN	dorsal Lateral geniculate nucleus	9.55	-13.95	8.26	40	5	R2
17	15	Pf#2	Nucleus parafascicularis thalami	1.85	-13.95	12.29	14	4	R3
18	16	Pcn	Nucleus paracentralis thalami	3.59	-12.15	14.59	5	2	R3
19	17	CM#2	nucleus centrum medianum (thalamus)	5.30	-14.85	14.87	30	2	R2
20	18	Csl	Nucleus centralis superior lateralis thalami	3.69	-13.95	19.39	10	2	R3
21	19	Cs#2	Nucleus centralis superior thalami	1.20	-9.00	20.40	5	1	R1
22	20	MI#1	Massa intermedia	0.00	-9.00	12.73	10	2	R1
23	21	SG	Nucleus suprageniculatus thalami	6.79	-17.78	11.39	5	4	R2
24	22	Li	Nucleus limitans thalami	3.69	-16.65	13.71	5	4	R2
25	23	Ret	Nucleus reticularis thalami	13.89	-18.00	15.68	118	2	R2
26	24	PIl-s	Nucleus pulvinaris inferior thalami, shell of the lateral subdivision	12.48	-18.00	11.31	2	5	R1
27	25	PIp	Nucleus pulvinaris inferior thalami, posterior subdivision	11.39	-18.90	12.73	5	5	R1
28	26	PIm	Nucleus pulvinaris inferior thalami, pars medialis	10.09	-18.45	12.08	5	5	R2
29	27	PIl	Nucleus pulvinaris inferior thalami, lateral subdivision	12.80	-18.45	12.51	5	5	R1
30	28	PIc	Nucleus pulvinaris inferior thalami, central subdivision	11.07	-18.00	11.86	5	5	R2

Data: A Pathak, SN Menon, and S Sinha, *Phys. Rev. E* **106**, 054304 (2022).

SPACE-INDEPENDENT PARTITIONING

How can we be sure that certain network properties, such as modular organization, are **not** simply a consequence of the underlying spatial embedding?

For this purpose, we need to redefine the modularity matrix $\mathbf{B}$ such that the expectation that a pair of nodes i and j are connected incorporates the distance d_{ij} between them.

For this, we follow the approach of Expert et al* and set

$$B_{ij} = A_{ij} - \frac{k_i^{in} k_j^{out} f(d_{ij})}{m},$$

where $f(d)$ is referred to as the the deterrence function, which defined as

$$f(d) = \frac{\sum_{i,j|d_{ij}=d} A_{ij}}{\sum_{i,j|d_{ij}=d} k_i^{in} k_j^{out}},$$

which is the weighted avg. probability that there is a link between nodes separated by a distance d.

In practice, this is computed by binning the distances and for each binned distance d_{bin} identifying all (i, j) pairs such that $d_{ij} = d_{bin}$ and obtaining $f(d_{ij}) = \Sigma_{i,j} A_{ij} / \Sigma_{i,j} k_i^{in} k_j^{out}$.

* P Expert, TS Evans, VD Blondel & R Lambiotte, *PNAS* **108**, 7663 (2011).

SPACE-INDEPENDENT PARTITIONING

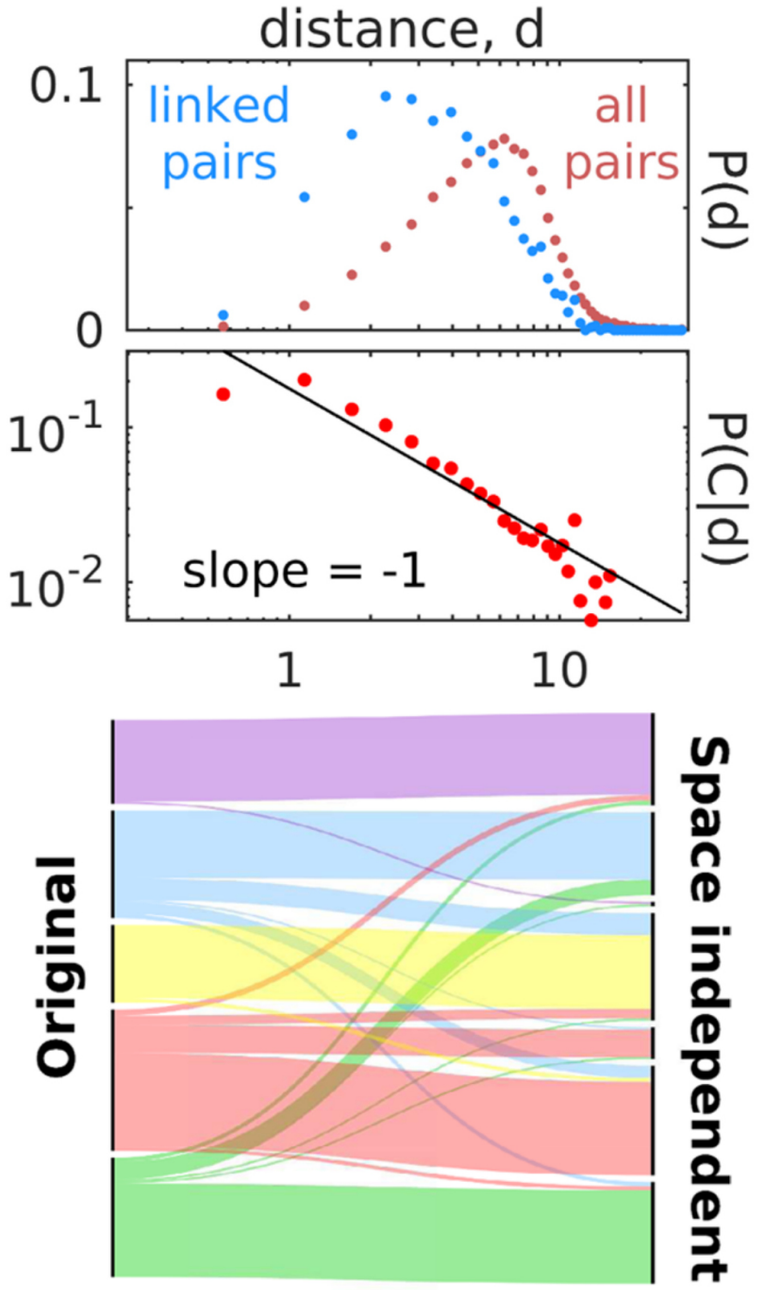

Simply considering the probability distribution of the distances between all linked pairs in the network we see that the values of d are much smaller that would be expected when looking at all pairs of nodes.

Similarly, considering the connection probability $P(C|d)$ between a pair of nodes separated by d, we see that it has a relationship $P(C|d) \sim d^{-1}$, demonstrating an explicit role of the spatial layout.

However, when determining the modules using the deterrence function, we see that the newly obtained modules strongly overlap with those obtained earlier.

Hence, physical proximity cannot provide a causal explanation for the modular structure.

images: A Pathak, SN Menon, and S Sinha, *Phys. Rev. E* **106**, 054304 (2022).

SPACE-INDEPENDENT PARTITIONING

If we compare the matrices A_{ij}, B_{ij} and d_{ij} we see that, despite discounting the effect of distance in identifying the modules, there is no significant difference between the distances between nodes within modules and across modules.

Here, the demarcation between the "space-independent" modules obtained by the modified approach are shown as white lines.

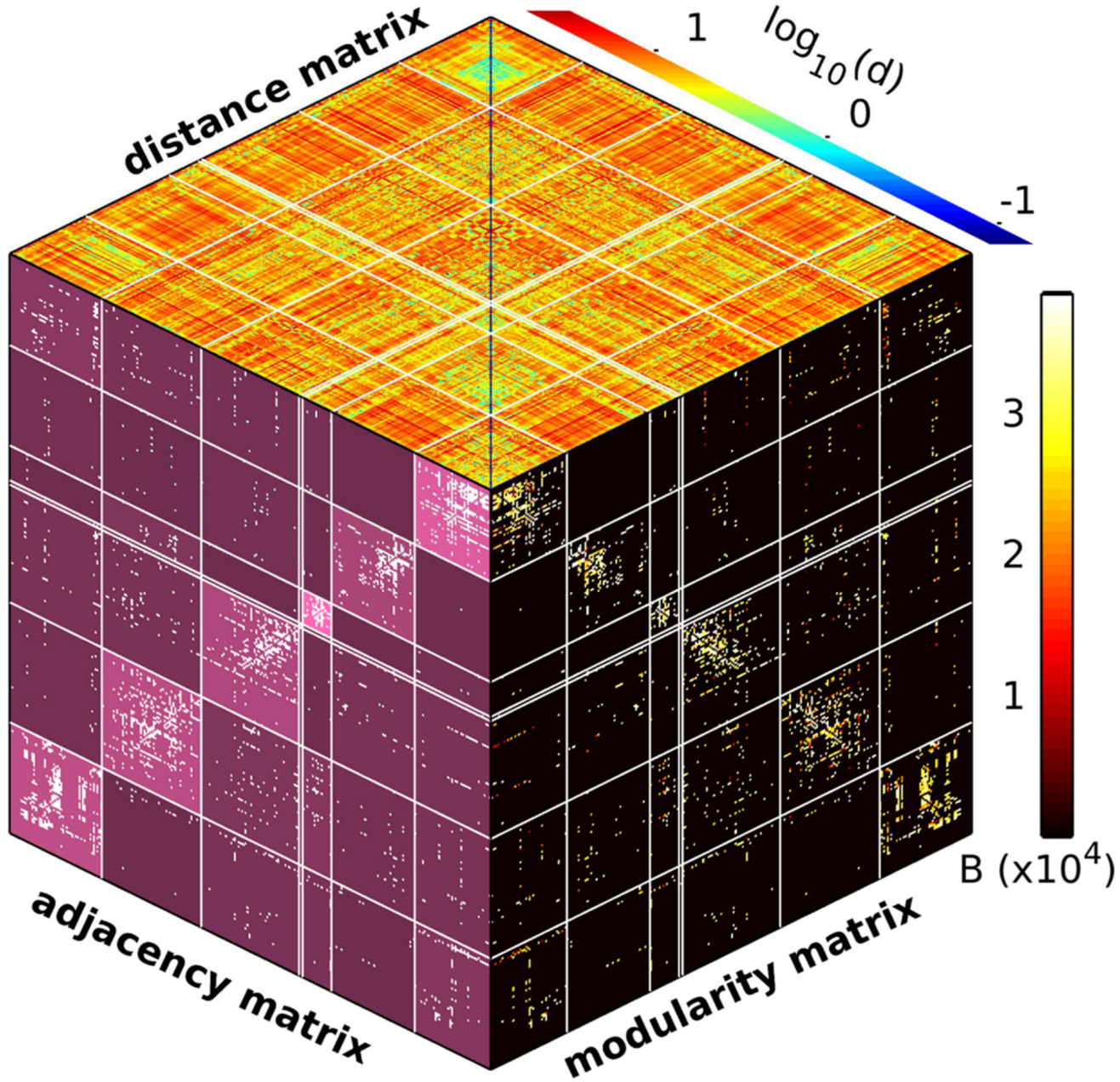

image: A Pathak, SN Menon, and S Sinha, *Phys. Rev. E* **106**, 054304 (2022).

COMPARING PARTITIONINGS

To quantify the similarity between modular decompositions $\{c_A\}_{i=1}^{M_A}$ and $\{c_B\}_{i=1}^{M_B}$ that yield M_A and M_B modules respectively in two distinct partitionings A and B of the same network, we use the normalized mutual information:

$$I_{norm}(A,B) = \frac{2\Sigma_i\Sigma_j P(c_i^A, c_j^B)\ln\left[P(c_i^A, c_j^B)/P(c_i^A)P(c_j^B)\right]}{-\Sigma_i P(c_i^A)\ln[P(c_i^A)] - \Sigma_j P(c_j^B)\ln[P(c_j^B)]}$$

where $P(c_i^X)$ is the probability that a randomly chosen node lies in module c_i^X and $P(c_i^A, c_i^B)$ is the joint probability that a randomly chosen node lies in both modules. The ratios of the relevant set sizes to the network size yields these probabilities.

When comparing the partitioning obtained with the original method vs the space-independent approach we expect that if the partitionings are identical then $I_{norm} = 1$, while $I_{norm} = 0$ implies maximum dissimilarity.

COMPARING PARTITIONINGS

To further establish that the obtained modular organisation is not primarily driven by the physical distance between areas, we generate three types of surrogate networks, specified by the dependence of the connection probability P between areas on the distance d between them:

1. distance-independent ($P \sim d^0$)
2. power-law dependence ($P \sim d^{-1}$)
3. exponential dependence ($P \sim \exp(-d)$)

We determine the resulting modules using the original and spatial dependent approaches, and calculate I_{norm}.

We find that for $P \sim d^0$ the values of I_{norm} are low since the identified modules arise through fluctuations alone. For $P \sim d^{-1}$ the value of I_{norm} obtained for the empirical network (arrow) is significantly larger than for the ensemble.

So, if the modules arisen *purely* from a distance-dependent constraint on connections, the partitionings obtained with the two approaches would be highly dissimilar.

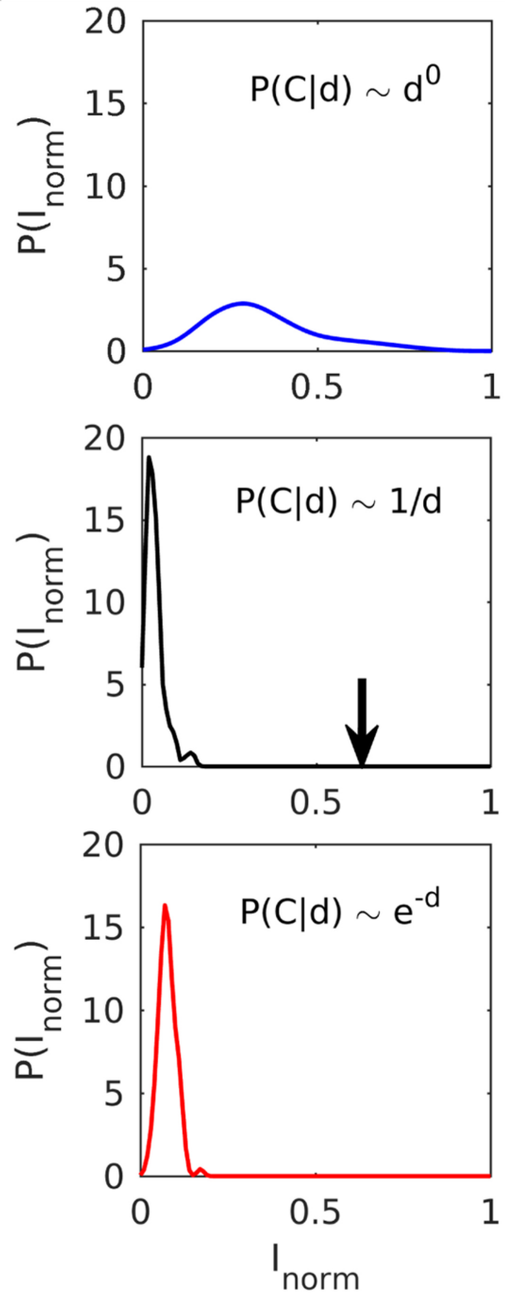

image: A Pathak, SN Menon, and S Sinha, *Phys. Rev. E* **106**, 054304 (2022).

COMPARING PARTITIONINGS

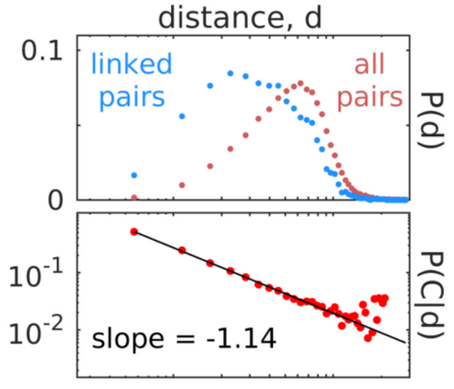

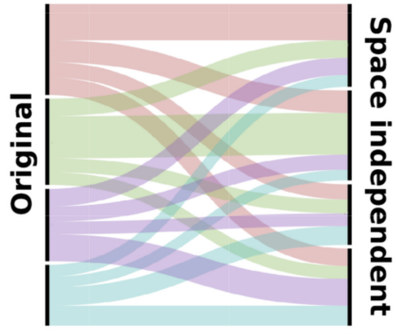

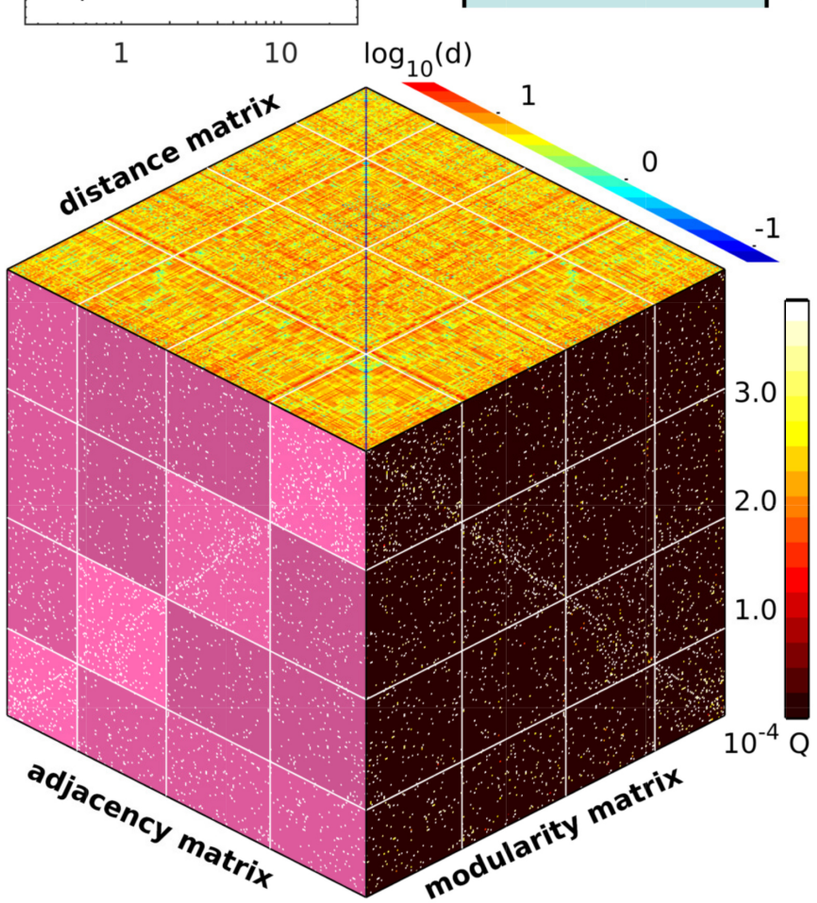

The dissimilarity between partitionings obtained for the two approaches is shown for a particular realisation.

For the ensembles with $P \sim d^0$, there is no difference in the distribution of Q values that can be obtained.

For those with $P \sim d^{-1}$, we see that the Q values for the empirical network are significantly higher.

For those with $P \sim \exp(-d)$, the deterrence function significantly nullifies the modularity.

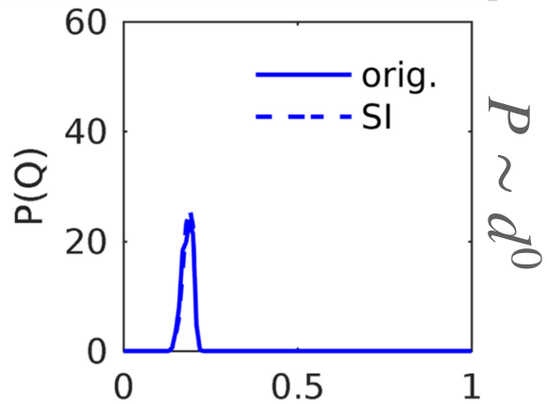

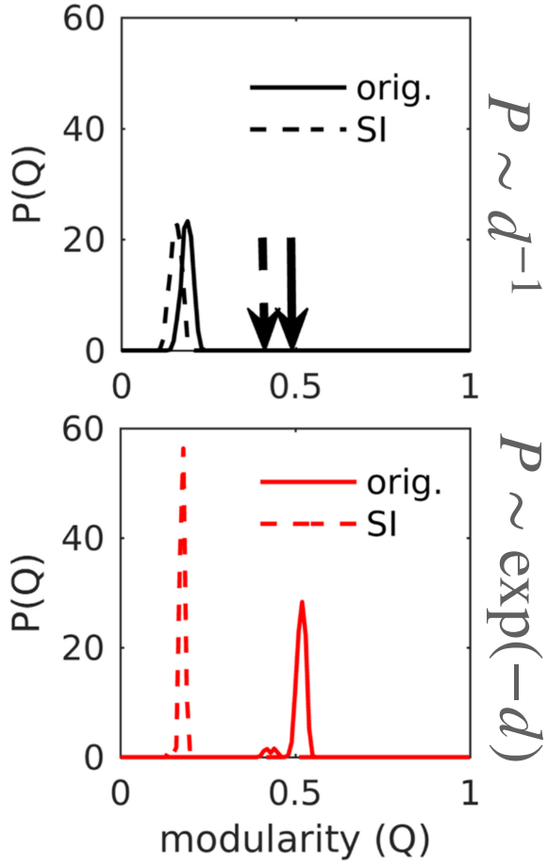

images: A Pathak, SN Menon, and S Sinha, *Phys. Rev. E* **106**, 054304 (2022).

CONCLUSIONS

A structural analysis of the macaque connectome reveals numerous interesting details:

- The specific modular organization of this connectome allows signals to spread very fast in contrast to equivalent networks with homogeneous distribution of connections.
- We find that this could possibly be understood because of observed properties such as R5 homophily, and the preference of connector hubs to link to peripheral nodes.
- The fact that almost all brain regions have similar distributions of functional categories suggests a uniformity of design that may embody a general computational logic.
- The overrepresentation of R5-R5 links is reminiscent of what has been observed for the C. elegans*, suggesting it might be a feature of networks that not only need to convey signals rapidly but also *process* them.

* RK Pan, N Chatterjee & S Sinha, *PLOS ONE* **5**, e9240 (2010).

CONCLUSIONS

- When considering the areas of the *Intraparietal Sulcus,* the AIP and MIP are (which coordinate motor tasks such as pointing) belong to module #2, while the LIP and VIP areas (which are involved in visual processing tasks such as saccadic eye movements) belong to module #5. Thus, functionalities of these areas tie in to the modules that they belong to. So, the module with which a particular brain area is associated may also alert us to possible functions of this area that have not yet been identified.

- The prefrontal and temporal parts of module #4 are known to have a role in social cognition in primates and correspond to the Broca's and Wernicke's areas in the human brain, respectively. It is hence an intriguing question as to whether some areas in module #4 developed from a common evolutionary precursor of the apparatus responsible for facilitating language in humans.

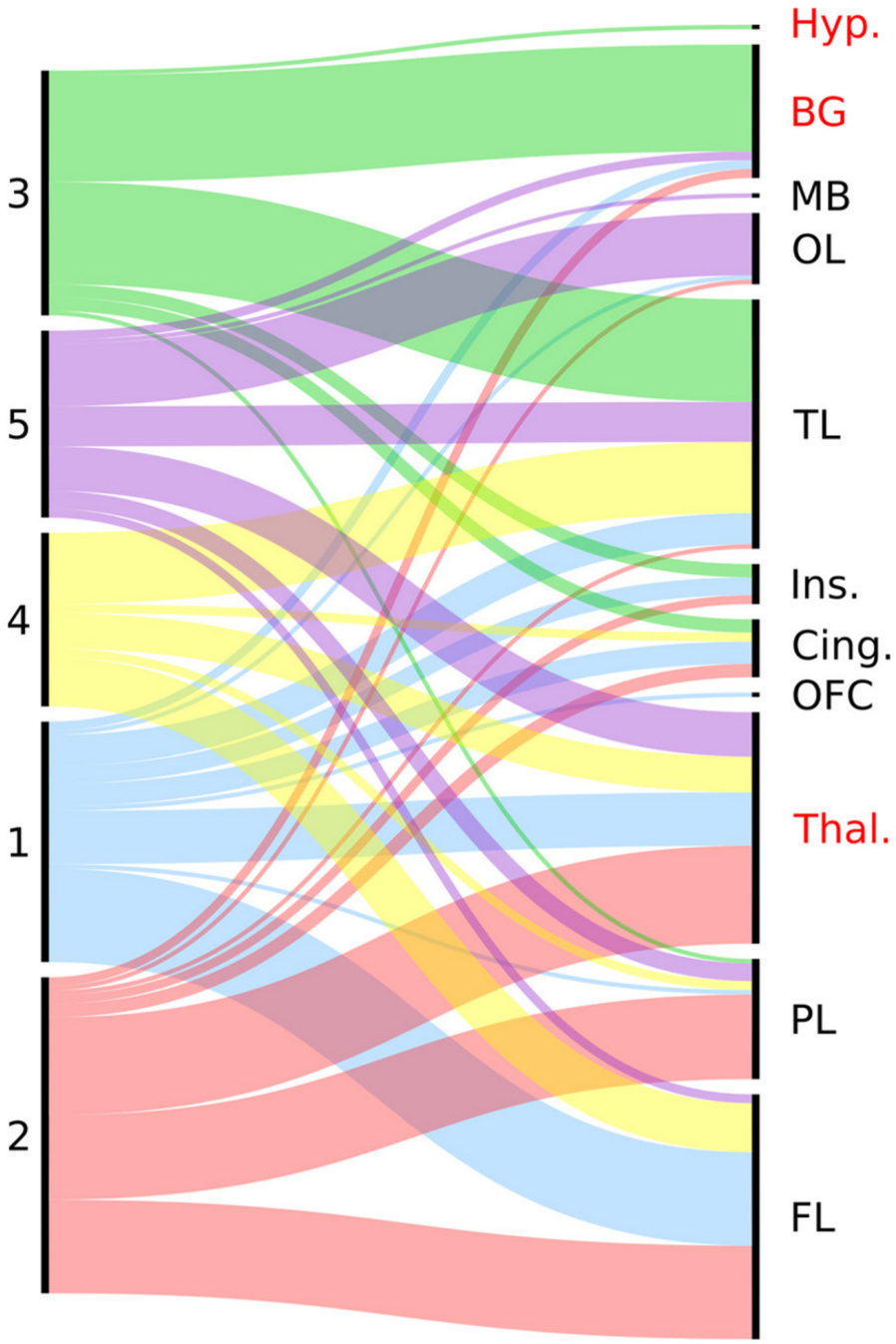

image: A Pathak, SN Menon, and S Sinha, *Phys. Rev. E* **106**, 054304 (2022).

FURTHER STUDY

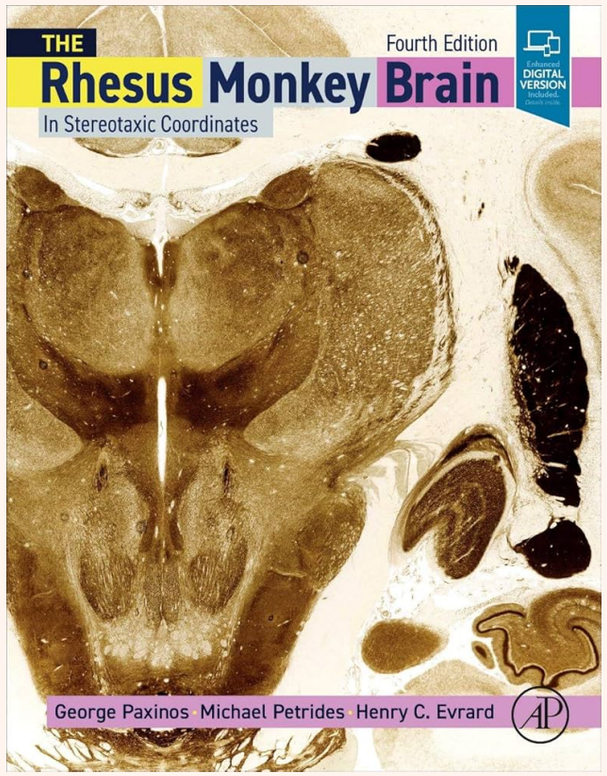

G Paxinos, XF Huang, and AW Toga,
The Rhesus Monkey Brain in Stereotaxic Coordinates
(Academic Press, 2000)

Scalable Brain Atlas website

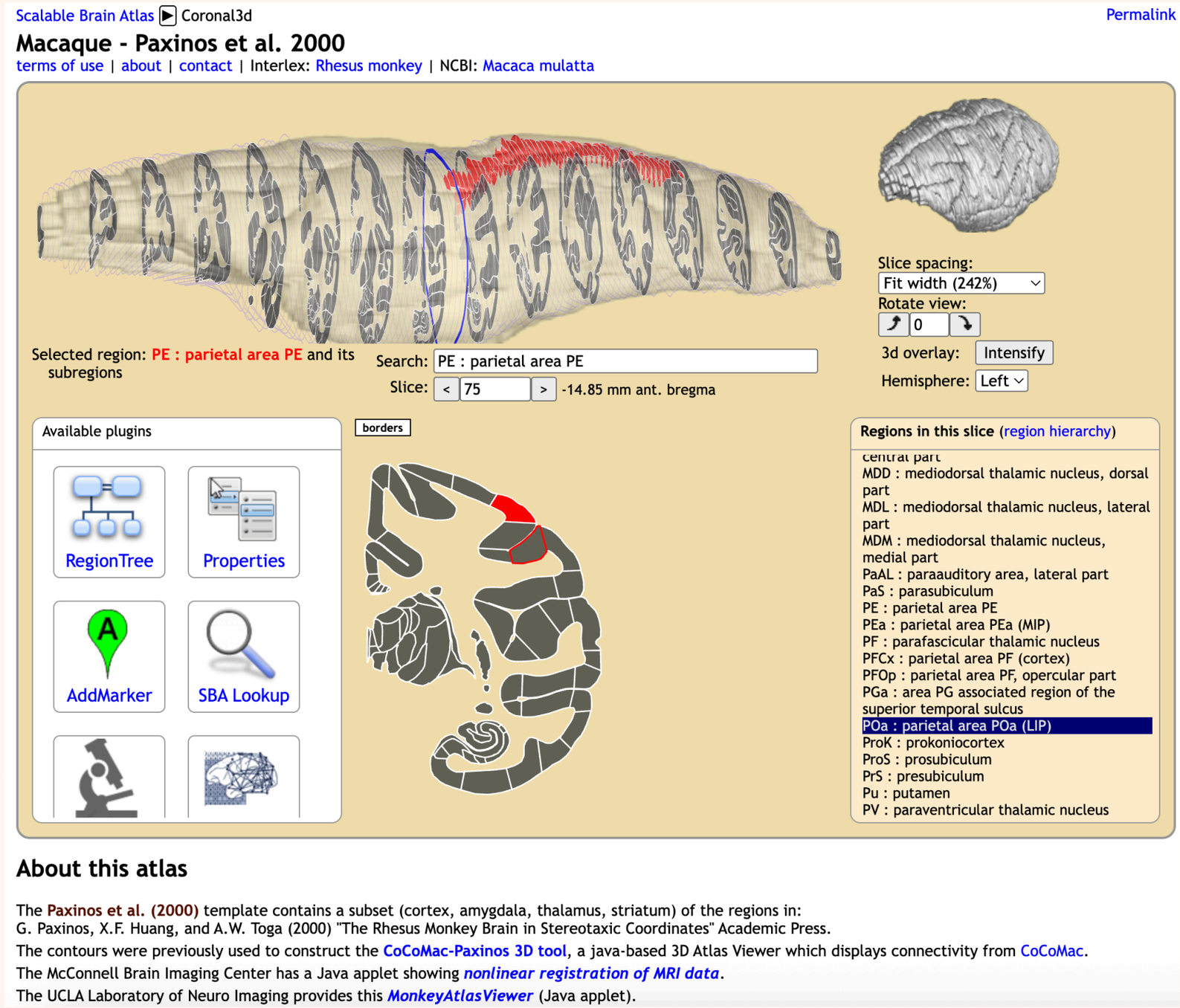

https://scalablebrainatlas.incf.org/macaque/PHT00

THANK YOU!

image: Steven Spielberg, "Indiana Jones and the Temple of Doom" (1984)